Late Cretaceous tectonothermal events of the Gangdese belt, southern Tibet

Xuxuan Ma, Zhiqin Xu, Alexander D Lusk, Saskia Erdmann, Xijie Chen, Shiwei Ma

Research Paper

GEOSPHERE

GEOSPHERE, v. 19, no. 3

https://doi.org/10.1130/GES02602.1

16 figures; 1 set of supplemental files

CORRESPONDENCE: xzq@nju.edu.cn; xuxuan.ma@hotmail.com

CITATION: Ma, X.X., Xu, Z.Q., Lusk, A.D., Erdmann, S., Chen, X.J., and Ma, S.W., 2023, Late Cretaceous tectonothermal events of the Gangdese belt, southern Tibet: Geosphere, v. 19, no. 3, p. 933–956, https://doi.org/10.1130/GES02602.1.

Science Editor: Andrea Hampel
Associate Editor: Francesco Mazzarini

Received 22 September 2022
Revision received 21 February 2023
Accepted 14 March 2023

Published online 20 April 2023

Late Cretaceous tectonothermal events of the Gangdese belt, southern Tibet

Xuxuan Ma[1,2,3], Zhiqin Xu[1,4,*], Alexander D. Lusk[5], Saskia Erdmann[6], Xijie Chen[7], and Shiwei Ma[1]

[1]Key Laboratory of Deep-Earth Dynamics of Ministry of Natural Resources, Institute of Geology, Chinese Academy of Geological Sciences, Beijing 100037, China
[2]National Observation and Research Station of Jiangsu Donghai Continental Deep Hole Crustal Activity, Donghai 222300, China
[3]Southern Marine Science and Engineering Guangdong Laboratory, Guangzhou 511458, China
[4]State Key Laboratory for Mineral Deposits Research, School of Earth Sciences and Engineering, Nanjing University, Nanjing 210046, China
[5]Department of Geoscience, University of Wisconsin–Madison, Madison, Wisconsin 53706, USA
[6]Institut des Sciences de la Terre d'Orléans (ISTO), Université d'Orléans, CNRS, BRGM, UMR 7327, F-45071 Orléans 53706, France
[7]Development and Research Center of China Geological Survey, Beijing 100037, China

ABSTRACT

The Gangdese belt of the southern Lhasa terrane (southern Tibet) records a Chilean-type accretionary orogeny driven by subduction of Neotethyan oceanic lithosphere, prior to Indo-Asian collision and formation of the Tibetan Plateau. We present detailed structural analysis of outcrops and a drill core in the Jiama copper ore district along with ^{40}Ar-^{39}Ar cooling ages from white mica, plagioclase, and potassium feldspar and zircon U-Pb geochronology of granitoids and sandstone. These data add new constraints to the formation of a major angular unconformity, deformation along and within the footwall of the Gangdese décollement, and the coupling between deformation and magmatism. Structural analysis indicates that top-to-the-south motion along the décollement produced south-vergent folding and thrusting of Upper Jurassic to Cretaceous strata in the Gangdese back-arc basin. A synthesis of new and compiled age data reveals that the décollement and associated south-vergent deformation occurred between ca. 90 and 65 Ma, contemporaneous with the formation of a major ca. 85–69 Ma angular unconformity between the overlying Paleocene–Eocene Linzizong Formation and the underlying Upper Cretaceous Shexing Formation. We posit that this deformation in the Gangdese belt resulted from flat-slab subduction of the Neotethyan oceanic slab beneath the southern margin of the Asian continent. A flat-slab subduction geometry is consistent with previously documented synchronous thrusting in the forearc and back-arc basins as well as the observed arc magmatic lull of the Gangdese belt between ca. 80 and 65 Ma.

INTRODUCTION

Orogenic belts are typically grouped into two broad categories: continent-continent collisional orogens and subduction-accretionary orogens (Uyeda and Kanamori, 1979; Stern, 2002; Grujic, 2006; Cawood and Buchan, 2007; Kellett et al., 2009). These two models are commonly end members, given that many orogens experience both continental collision and oceanic subduction during their evolution (Yin and Harrison, 2000; Jolivet et al., 2016; Kapp and DeCelles, 2019; van Hinsbergen et al., 2019). For example, the Tibetan-Himalayan orogen is typically considered a prototypical continent-continent collisional orogen and has received paramount attention within the geological community (Molnar et al., 1993; Tapponnier et al., 2001; Royden et al., 2008; Labrousse et al., 2010; Grujic et al., 2020; Carosi et al., 2013, 2018; Jamieson and Beaumont, 2013; Xu et al., 2013; Li et al., 2015a; Ding et al., 2016). However, during the Mesozoic, the southern margin of the Lhasa terrane was subject to a period of accretionary subduction prior to the Indo-Asian continental collision (Ratschbacher et al., 1992; Aitchison et al., 2000; Zhao et al., 2021), which may have resembled the present-day tectonic configuration of the South American Andes (Manea et al., 2017).

Subduction-accretionary orogens form curvilinear belts of magmatic and accreted material above sites of subducting oceanic lithosphere (Cawood and Buchan, 2007). Broadly speaking, subduction-accretionary orogens can also be subdivided into two end-member categories: those in which the orogen is under compression and those in which it is under extension. These two end members have been termed "Chilean type" and "Mariana type," respectively, by Uyeda and Kanamori (1979). "Chilean-type" orogens tend to be characterized by widespread crustal shortening and uplift, including the development of fold-thrust systems in forearc and retro-arc regions, in conjunction with episodic arc magmatism (DeCelles et al., 2015; Ducea et al., 2015; Paterson and Ducea, 2015). Arc-continent accretion and arc magmatism are highly episodic, with magmatic activity commonly characterized by flare-ups and lulls (Attia et al., 2020; Ma et al., 2022). However, in the case of subduction-accretionary orogens, the driving mechanisms of formation are less obvious compared to continent-continent collisional orogens. Still debated are the crust-mantle–scale processes that drive the formation of accretionary orogens and the role of these processes in the episodic

Xuxuan Ma https://orcid.org/0000-0001-9847-9109
*xzq@nju.edu.cn

nature of deformation and magmatism (Paterson and Ducea, 2015).

The Lhasa terrane (southern Tibet), which was accreted to the southern margin of the Eurasian continent, not only records the final Indo-Asian collision processes but also preserves evidence for the subduction of the Neotethyan oceanic slab (Wen et al., 2008a; Kapp and DeCelles, 2019; Zhu et al., 2019; Ma et al., 2021a). However, much of the Mesozoic evolution remains poorly understood, in part due to structural and magmatic modification during the Cenozoic (Metcalf and Kapp, 2019; Sundell et al., 2021). The Gangdese arc magmatic belt, exposed along the southern margin of the Lhasa terrane (Fig. 1A), is inferred to have formed during the subduction of Neotethyan oceanic lithosphere beneath the Lhasa terrane, antecedent to the collision of the Indian and Asian continents at ca. 60–55 Ma (DeCelles et al., 2014; Hu et al., 2015).

The tectonic regime that prevailed during the Late Cretaceous along the southern margin of the Lhasa terrane is still debated. Some models suggest that Late Cretaceous to Paleogene shortening of the Lhasa terrane may have been punctuated by a 90–70 Ma phase of extension that led to the rifting of a southern portion of the Gangdese arc, with the opening of a back-arc ocean basin (Kapp and DeCelles, 2019; Sundell et al., 2021). Alternative models invoke Late Cretaceous crustal deformation in the back-arc and forearc basins of the Gangdese magmatic arc that is associated with the accretionary stage of the Tibetan-Himalayan orogeny (Kapp et al., 2007; Ma et al., 2017a). In other words, the Gangdese belt may have experienced a "Chilean-type" orogeny during the Late Cretaceous (Wen et al., 2008b; Ding et al., 2014; Dong et al., 2018; Zhu et al., 2019). The two competing end-member hypotheses for the Late Cretaceous tectonic evolution of the southern Lhasa terrane require reexamination. However, studies of the tectonic structures and their evolution are still scarce (Kapp et al., 2007; Ma et al., 2017a; Wang et al., 2017a). More importantly, the temporal relationship between deformation and the episodic magmatism of the Gangdese belt (namely the arc magmatic tempos) remains largely unexplored. These relationships are key for understanding tectonic-scale driving forces and for modeling the thermal-structural evolution of orogens from early-stage accretion to late-stage continental collision.

The central part of the Gangdese belt, specifically the region between Lhasa and Mozhugongka, exposes Lower Jurassic to lower Eocene volcano-sedimentary sequences as well as voluminous intrusive rocks, including the Paleocene Quxu batholith (Figs. 1 and 2). Rocks exposed in this region therefore preserve a record of the structural evolution of the Late Cretaceous accretionary orogeny along with their relation to the magmatic tempos of the Gangdese batholith. Here, we present new structural observations from field outcrops and a drill core as well as geochronological data to characterize the tectonic framework and deformation of the Gangdese back-arc basin. We also explore the relationship between the episodic magmatism and tectonics during the accretionary orogenic phase. Our work sheds new light onto the processes and timing of accretionary orogenesis of the Lhasa terrane prior to the Indo-Asian collision and furthers our understanding of coupled continent-continent collisional and accretionary-subduction orogeny.

GEOLOGICAL BACKGROUND

The Gangdese magmatic belt, located at the southern margin of the Lhasa terrane, extends for >1500 km along strike, with a width ranging between ~20 and 100 km (Fig. 1A). To the west, the Gangdese magmatic belt is linked to the Ladakh and Kohistan batholiths. To the east, it is linked to the Lohit batholith (Zhu et al., 2019). The Gangdese magmatic belt is composed primarily of large-scale batholiths and corresponding volcanic sequences, preserving a record of Neotethyan oceanic slab subduction from the Mesozoic to Cenozoic (Yin and Harrison, 2000; Ji et al., 2009; Hu et al., 2015; Najman et al., 2017; Li and Mattern, 2021). Compositionally, the Gangdese batholith comprises gabbro, diorite, granodiorite, monzogranite, and granite as well as porphyry stocks, ranging in age from Middle Triassic (ca. 240 Ma) to late Miocene (ca. 9.5 Ma) (Laskowski et al., 2018; Meng et al., 2018; Ma et al., 2020). Two dominant age peaks are interpreted to correspond to two magmatic flare-ups at 90 ± 5 Ma and 50 ± 3 Ma (Zhu et al., 2019). Two contrasting tectonic models have been widely used to interpret the Late Cretaceous magmatic flare-up: slab rollback and ridge subduction of the Neotethyan oceanic lithosphere beneath the Lhasa terrane (Ma et al., 2015; Zhu et al., 2019; Meng et al., 2021; Ding et al., 2022a). The second magmatic flare-up that peaked ca. 50 Ma could have been caused by the slab breakoff of the subducted Neotethyan oceanic lithosphere (Zhu et al., 2015, 2019).

Volcano-sedimentary sequences that are spatiotemporally associated include the Lower to Middle Jurassic Bima and Yeba Formations, the Upper Jurassic Duodigou Formation, the Lower Cretaceous Linbuzong and Chumulong Formations, and the Upper Cretaceous Shexing Formation, among others (Figs. 1 and 3). The Bima Formation comprises basalt, basaltic andesite, andesite, rhyolite, limestone, and slate (Kang et al., 2014; Wang et al., 2016; Ma et al., 2017b). The Yeba Formation is characterized by bimodal volcanic rocks whose formation is attributed to back-arc rifting that was triggered by the northward subduction of the Neotethyan oceanic slab (Zhu et al., 2008a; Liu et al., 2018; Ma et al., 2019). The Duodigou Formation is dominantly limestone. The Lower Cretaceous Linbuzong and Chumulong Formations comprise chiefly slate and siltstone, and the Upper Cretaceous Shexing Formation comprises siltstone and sandstone. The variable lithologies imply a regressive depositional environment.

Tectonically, the Gangdese magmatic belt is bound to the north by the Luobadui-Milashan fault zone and by the Indus–Yarlung Tsangpo suture zone to the south (Fig. 1A) (Pan et al., 2006; Zhu et al., 2008b). The Luobadui-Milashan fault zone exposes a stack of folded, north-directed thrust faults, ~15 km north of the Linzhou area, including the Gulu-Hamu retro-arc thrust, which records northward translation of the Gangdese belt over the Central Lhasa subterrane (Murphy et al., 1997; Kapp et al., 2007). The structurally highest of these thrusts, with Paleozoic strata in the hanging wall, is intruded by a suite of 57–50 Ma granitoids along strike to the west (Kapp et al., 2007). To the north of the Luobadui-Milashan fault zone, the Central Lhasa subterrane is characterized by Precambrian basement intruded by

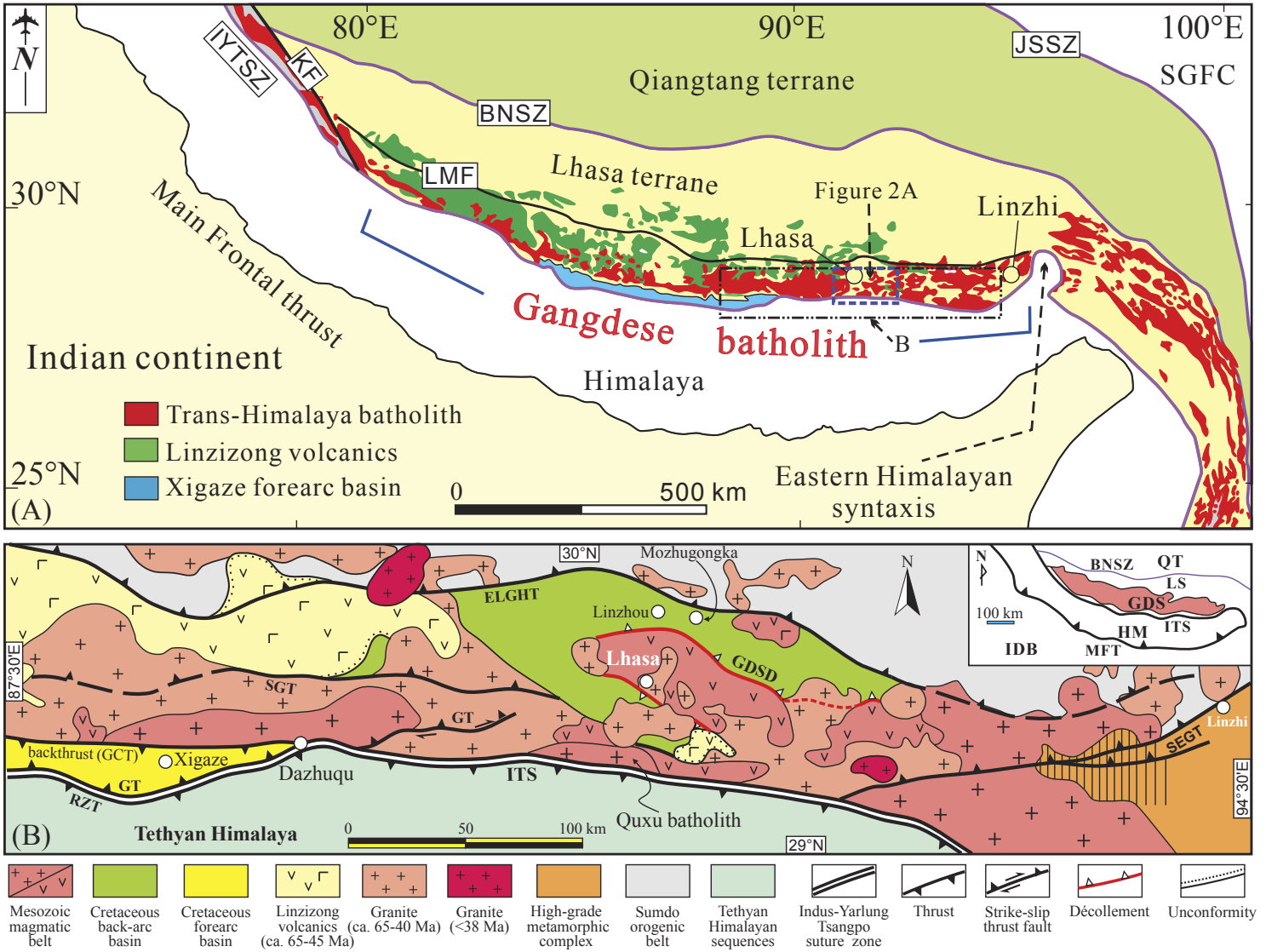

Figure 1. (A) Tectonic framework of the Lhasa terrane and location of the Gangdese magmatic belt in the context of the southern Tibetan Plateau (Zhu et al., 2019), which is composed of, from north to south, the Songpan-Ganze, Qiangtang, Lhasa, and Tethyan Himalaya terranes. The extent of the Gangdese batholith and the exposure of the Linzizong Formation volcanic succession are from Chung et al. (2005). BNSZ—Bangong-Nujiang suture zone; IYTSZ—Indus–Yarlung Tsangpo suture zone; JSSZ—Jinsha suture zone; KF—Karakoram fault; LMF—Luobadui-Milashan fault; SGFC—Songpan-Ganze flysch complex. (B) Schematic tectonic map of the central-eastern Gangdese tectono-magmatic belt of the southern Lhasa terrane (modified from Yin et al., 1994; Kapp et al., 2007; Ma et al., 2017a), showing the Gangdese décollement, which is located to the south of the retro-arc fold-thrust belts (Emei La–Gulu-Hamu thrust) and to the north of the Gangdese thrust. QT—Qiangtang terrane; LS—Lhasa terrane; HM—Himalaya terrane; IDB—Indian block; GDS—Gangdese magmatic belt; ITS—Indus–Yarlung Tsangpo suture zone; MFT—Main Frontal thrust; RZT—Renbu-Zedong thrust; GCT—Great Counter thrust; GT—Gangdese thrust; SGT—Southern Gangdese thrust; ELGHT—Emei La–Gulu-Hamu thrust; GDSD—Gangdese décollement; SEGT—Southeastern Gangdese thrust.

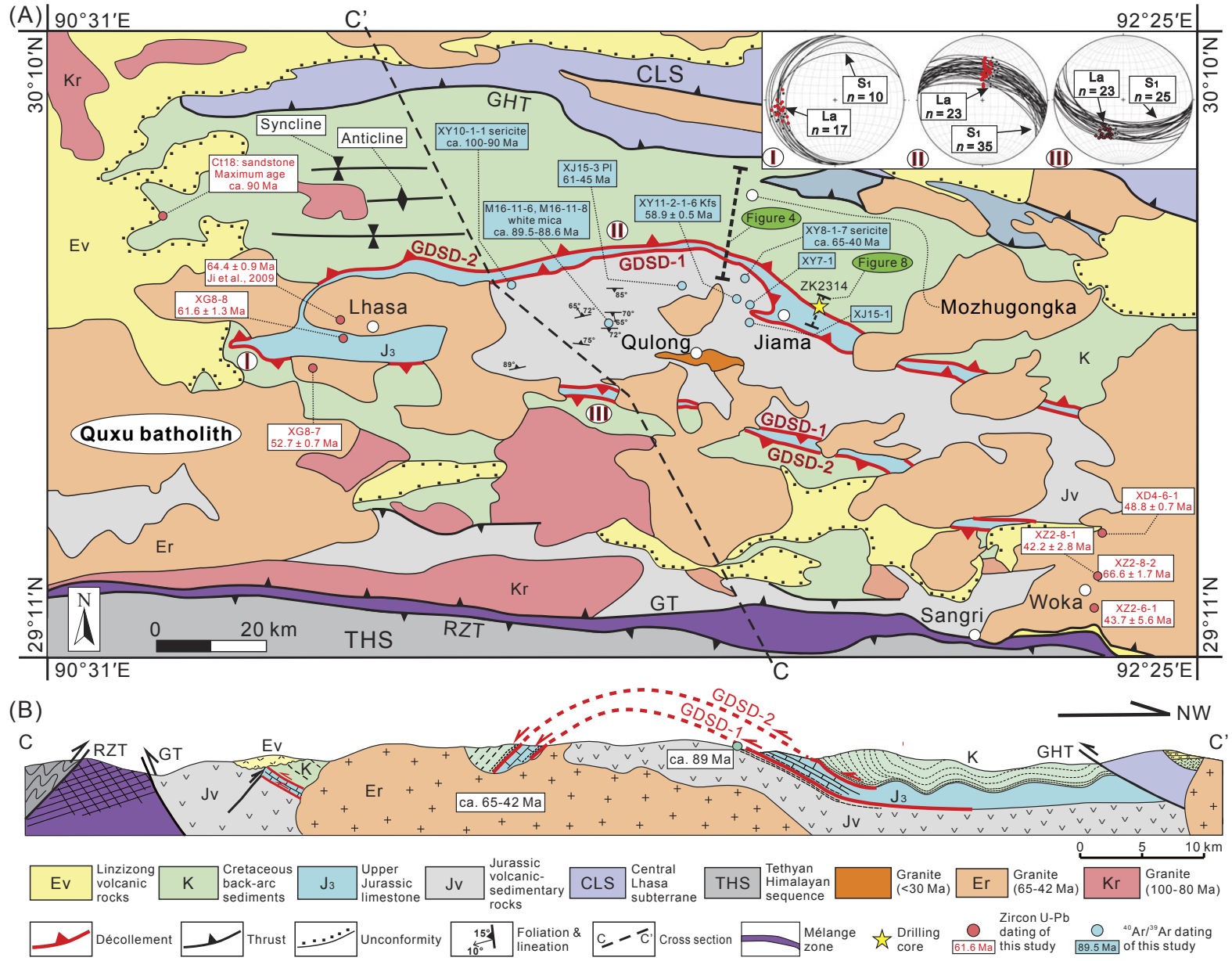

Figure 2. Schematic tectonic map (A) and cross section (B) of the Gangdese back-arc basin of the southern Lhasa terrane with published age data and our new age data, accompanied by sample locations. The map area of A is outlined in Figure 1A. Shown is the top-to-the-south Gangdese décollement (GDSD), which is composed of (1) the lower décollement layer (GDSD-1) between the overlying Upper Jurassic Duodigou Formation limestone and the underlying Middle Jurassic volcanic rocks of the Yeba Formation and (2) the upper décollement layer (GDSD-2) between the overlying Lower Cretaceous Linbuzong Formation and the underlying Upper Jurassic Duodigou Formation limestone. The GDSD was uplifted to form a dome structure with outward-dipping foliation and stretching lineation. The upper-right insets in A show lower-hemisphere, equal-area projections of foliation (S_1) and stretching lineation (La) orientations of the Lhasa dome structure. Foliation and lineation in inset I were collected from the western flank of the Lhasa dome, with foliation dipping to the west. Foliation and lineation in inset II were collected from the northern flank of the Lhasa dome, showing foliation dipping to the north. Foliation and lineation in inset III were collected from the southern flank of the Lhasa dome, showing a south-dipping foliation. RZT—Renbu-Zedong thrust; GT—Gangdese thrust; GHT—Gulu-Hamu thrust; Pl—plagioclase; Kfs—K-feldspar.

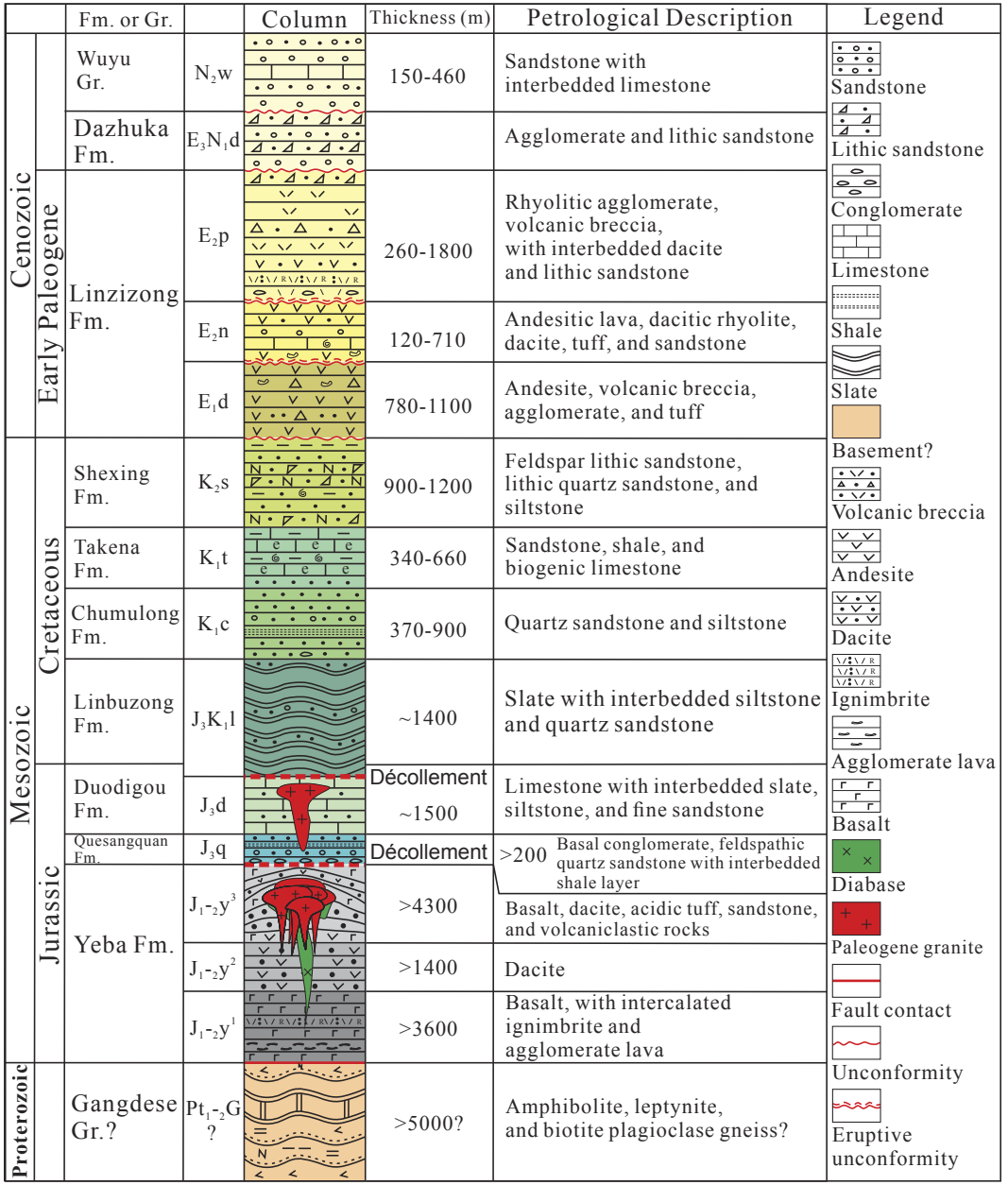

Figure 3. Stratigraphic column for the volcano-sedimentary sequences in the central Gangdese belt, southern Tibet. All of the volcano-sedimentary sequences in Figures 1B and 2 are presented in this stratigraphic column. In the column to the right of the formation/group column are the markers or codes of stratigraphic sequences designated by local geologists. Notations represent different parts of the series/epochs for each stratus. This column is modified from Ma et al. (2019).

voluminous Jurassic–Cretaceous, collision-related S-type granites (Zhu et al., 2008b). In contrast, the Gangdese belt is characterized by juvenile crust, apparently lacking basement rocks (Ji et al., 2009). In addition, the Triassic–Jurassic igneous rocks of the Gangdese belt show highly depleted zircon Lu-Hf and whole-rock Sr-Nd isotopic signatures and arc-like geochemical composition indicative of continued subduction of the Neotethyan oceanic lithosphere (Zhu et al., 2008b; Wang et al., 2016; Ma et al., 2020).

The Xigaze forearc basin, immediately north of the Indus–Yarlung Tsangpo suture zone (Fig. 1B), is composed of the Xigaze Group, including the Ngamring, Padana, and Qubeiya Formations, deposited at ca. 107–65 Ma (Wu et al., 2010; Orme et al., 2015). To the north, the Xigaze forearc basin is bound by the south-dipping Great Counter thrust, which is of late Oligocene–early Miocene age (Fig. 1B) (Yin, 2006; Laskowski et al., 2017). To the south, the basin is defined by the north-dipping Gangdese thrust, which is thought to have initiated during the late Oligocene (Yin et al., 1994). Forearc and subsequent syn-collisional sequences were deposited on the Xigaze ophiolitic basement (Huang et al., 2015; Orme and Laskowski, 2016; Wang et al., 2017b). Further to the south, a sedimentary-matrix mélange was thrust southward over the southern Tethyan Himalayan sequence along the east-west–striking Zhongba-Gyangze thrust at ca. 71–61 Ma (Ding et al., 2005; Wang et al., 2017a).

The Late Cretaceous Gangdese back-arc basin (~200 km in length and ~60–70 km in width) is located at the northern side of the Mesozoic Gangdese batholith, north of the Quxu batholith (Fig. 1B). The basin exposes marine sedimentary rocks of the Upper Jurassic Duodigou Formation and terrestrial sedimentary rocks of the Cretaceous Linbuzong, Chumulong, Takena, and Shexing Formations (Figs. 2 and 3) totaling a thickness of ~3 km. The basement of the basin consists of basic and intermediate volcanic rocks of the Yeba Formation with ages between 190 and 174 Ma (Fig. 3) (Zhu et al., 2008a). Back-arc sequences are overlain by the ca. 65–45 Ma Linzizong Formation volcanic succession along an angular unconformity (hereon referred to as the Gangdese angular unconformity) (Mo et al., 2007; Zhu et al., 2015). Below the unconformable contact, the Gangdese back-arc sequences are strongly folded, whereas the overlying Linzizong volcanic sequences remain weakly deformed (Kapp et al., 2007).

STRUCTURAL OBSERVATIONS

Based on detailed field investigation, we distinguish two episodes of overprinting deformation. The first deformation phase (D_1) is contractional, accommodated by folding and south-vergent thrusting. The second phase of deformation (D_2) is also contractional and expressed as regional doming and open folding of D_1 structures.

First Deformation (D_1)—Gangdese Décollement

D_1 is defined by a series of folds and south-vergent thrusts developed in the Upper Jurassic to Lower Cretaceous strata of the Gangdese back-arc basin (Fig. 4). Fold axial traces strike east-west and

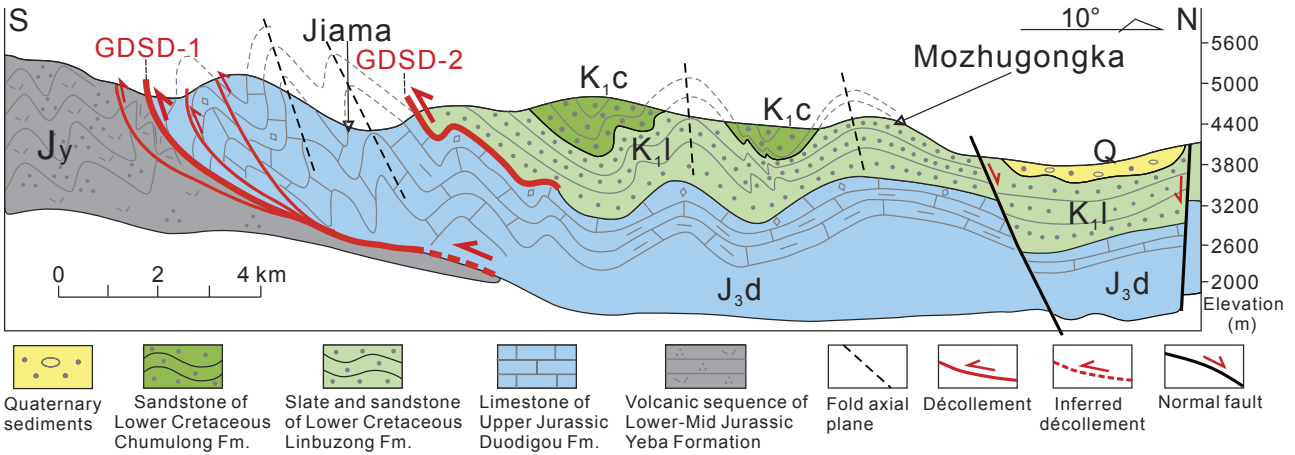

Figure 4. Cross-section profile from the Jiama mine to Mozhugongka County illustrating the Gangdese décollement (GDSD) and the Upper Jurassic to Cretaceous strata of the Gangdese back-arc basin. See Figure 2A for cross-section location. Jy—Middle Jurassic Yeba Formation; J_3d—Upper Jurassic Duodigou Formation; K_1l—Lower Cretaceous Linbuzong Formation; K_1c—Lower Cretaceous Chumulong Formation; Q—Quaternary sediments; GDSD-1—lower décollement layer of the GDSD; GDSD-2—upper décollement layer of the GDSD.

axial planes are characterized by upright orientations in the upper strata and by south-verging open folds in the stratigraphically lower strata (Fig. 4; Fig. S1 in the Supplemental Material[1]). Formation of the south-vergent structures is inferred to be associated with a ~2-km-thick composite sole detachment zone, exposed between the underlying Middle Jurassic Yeba Formation sequence and the overlying Upper Jurassic–Cretaceous sediments. We refer to these structures as the Gangdese décollement (GDSD) (Figs. 2B and 4). The GDSD includes two décollement surfaces. The lower décollement surface (GDSD-1) includes a ~500-m- to ~1-km-thick mylonite zone developed within volcanic and sedimentary rocks of the underlying Middle Jurassic Yeba Formation and overlying Upper Jurassic limestone of the Duodigou Formation (Fig. 5). The upper décollement surface (GDSD-2) is composed of a 1.5–2-km-thick shear zone developed in slate and sandstone between the underlying Upper Jurassic Duodigou Formation limestone and the overlying Lower Cretaceous Linbuzong Formation slate and sandstone (Fig. 4). Despite shearing and inferred displacement along the décollement, the original stratigraphy remains intact. We suggest that the upper and lower contacts of the Upper Jurassic Duodigou Formation limestone localized strain, promoting formation of the two décollement surfaces.

The mylonitic sandstone and schist of GDSD-1 are characterized by north-dipping foliation (S_1) and north-south–trending stretching lineation (L_1) (Figs. 5A and 5B). The north-south–trending stretching lineation is defined by stretched volcanic clasts, felsic mineral clusters, and plagioclase clasts (Fig. 5D). S-C fabric orientation and asymmetric volcanic clasts within the mylonitized volcanic rocks indicate dominantly top-to-the-south and/or top-to-the-southeast sense of shear (Figs. 5A–5C). Top-to-the-south and/or top-to-the-southeast shearing of GDSD-1 is further evidenced by asymmetric tails on feldspar clasts, asymmetric calcite, S-C fabric orientation, and felsic boudins or lenses (Figs. 6 and 7).

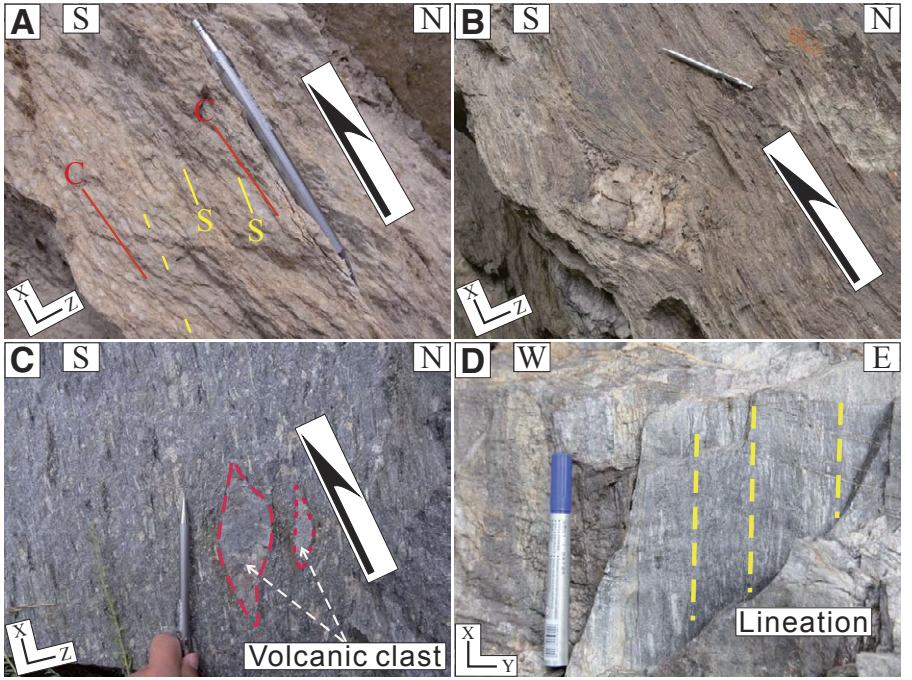

Figure 5. Deformation structure in the field. (A and B) Deformed schist, whose protolith was the sandstone of the Yeba Formation. The quartz veins and/or boudins have been rotated into sigma-type blocks, showing top-to-the-south and/or top-to-the-southeast shearing. Lines of C and S represent two sets of planar structures, a shear surface (C) and a foliation (S). (C) Field photo of deformed volcanic rocks of the Yeba Formation showing top-to-the-south and/or top-to-the-southeast shearing, where volcanic clasts have been rotated into sigma-type blocks. The deformed planes show highly vertical angles, which could have been caused by the later doming process due to pluton intrusion. (D) Mineral lineation defined by plagioclase, felsic mineral assemblages, and volcanic clasts within the schist.

Rocks deformed within GDSD-2 record similar structures and kinematics to those in GDSD-1. In outcrop, S-C fabrics, asymmetric porphyroclasts, and folds are consistent with top-to-the-south sense of shear (Ma et al., 2017a). In thin section, deformed rocks from the GDSD-2 zone show asymmetric feldspar, calcite, and biotite clasts (Fig. 6B), S-C fabrics (Fig. 6C), and sigma-type felsic lenses (Fig. 6D) also consistent with these kinematics.

Rocks deformed by GDSD-2 were found in drill core ZK2314, drill line 23, in the central segment of the Jiama mining district (Figs. 2 and 8), northeast of Lhasa. The ZK2314 drill core recovered 311.2 m, which included Lower Cretaceous Linbuzong sandstone and slate (core depths of 0–220 m), a porphyry zone (220–230 m), and Upper Jurassic marble or limestone of the Duodigou Formation (240–311.2 m) (Fig. 9). The porphyry Cu ore body intruded along the shear zone of GDSD-2 at 16–15 Ma (Fig. 8), indicating that deformation along the shear zone had ceased by that time (Yang et al., 2016).

[1]Supplemental Material. Ar-Ar dating results of mylonite, zircon U-Pb dating results of granites, and detrital zircon U-Pb dating results of Shexing Formation sandstone, as well as magmatic and detrital zircon U-Pb ages and Hf isotopes from many other published papers. Includes additional figures, as well as detailed analytical methods. Please visit https://doi.org/10.1130/GES.S.22321042 to access the supplemental material, and contact editing@geosociety.org with any questions.

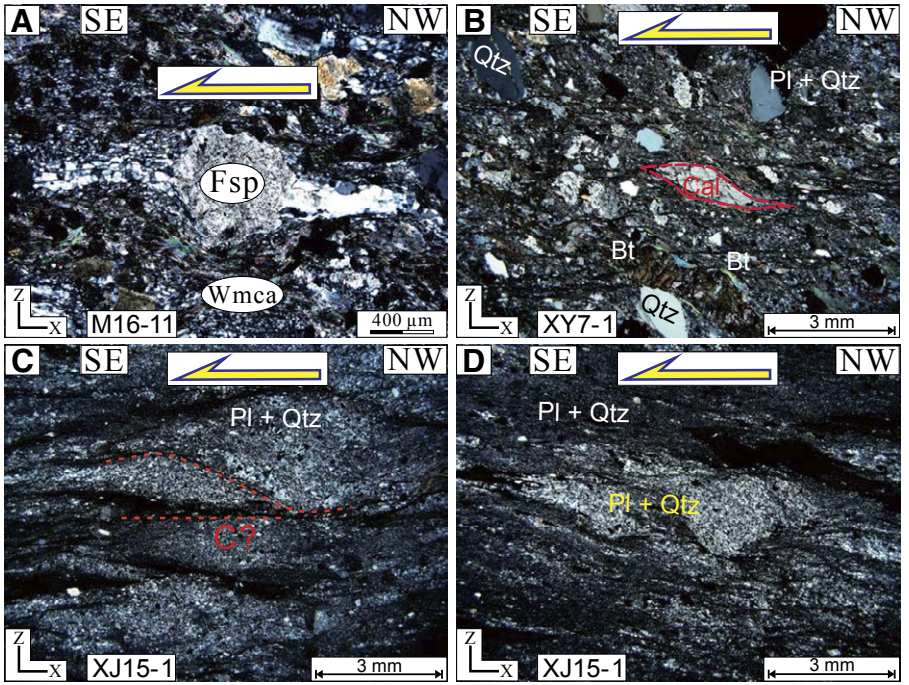

Figure 6. Photomicrographs of samples from the lower décollement layer of the Gangdese décollement (GDSD-1) showing top-to-the-southeast shearing recorded by sigmoidal feldspars with quartz tails (A), rotated calcite (B), S-C fabric (C), and sigma-type felsic boudins and lenses (D) from mylonites of the top part of the Middle Jurassic Yeba Formation volcano-sedimentary rocks and the base part of the Upper Jurassic Duodigou Formation limestone. Bt—biotite; Cal—calcite; Fsp—feldspar; Pl—plagioclase; Qtz—quartz; Wmca—white mica.

Slate and sandstones of the Lower Cretaceous Linbuzong Formation (0–220 m of drill core ZK2314) record evidence for ductile deformation including foliation and cleavage development (S_1), grain-size reduction (which we interpret to result from dynamic recrystallization), shear-band development, and folding of quartz veins (Figs. 9 and 10). Microstructures recorded within the drill core either are consistent with top-to-the-south and/or top-to-the-southeast sense of shear or are ambiguous and do not contain convincing shear-sense indicators. In parts of the drill core, asymmetric folding could be suggestive of top-to-the-north sense of shear, opposite that of GDSD kinematics (Figs. 9 and 10). The Upper Jurassic limestone of the Duodigou Formation (240–311.2 m of ZK2314) is characterized by grain-size reduction, development of a gently north-dipping foliation, and a NNE-SSW–trending stretching lineation (Figs. 9 and 10).

We posit that the deformation of the Cretaceous Linbuzong and Shexing Formations (Fig. S1E), recorded by the south-vergent structures with upright folds in the top and tight to isoclinal folds with north-dipping axial planes in the lower part, is associated with the sole GDSD-2 décollement (Fig. 9). In contrast, the Paleogene Linzizong Formation volcanic sequence is weakly deformed and unconformably overlies on the intensely deformed Shexing Formation (Fig. S1E; Kapp et al., 2007).

Second Deformation (D_2)—Folding and Doming

The GDSD was folded into open, generally upright to slightly south-vergent folds and formed a kilometer-scale dome structure. Radiating orientations of the S_1 foliation and stretching lineation were observed in the Jurassic Yeba and Duodigou Formations in the Lhasa region, providing evidence for this separate deformational event (Fig. 2A). The northern and southern flanks of the anticline show steeply north-dipping and south-dipping foliation orientations, respectively, whereas the western flank records foliation orientations gently dipping to the west (10°–30° dip) accompanied by an east-west–trending lineation orientation (Figs. 2A and 2B). This domal structure was previously named the "Lhasa dome" (Ma et al., 2017a). The steep to nearly vertical dips recorded by the Yeba Formation may result from steepening of S_1 due to doming (Fig. 5). We tentatively propose that the cryptic, and in some cases ambiguous, top-to-the-north shear sense indicators recorded in parts of the drill core could be associated with formation of the Lhasa dome, given that timing estimates overlap.

GEOCHRONOLOGY

To constrain the timing of the Gangdese accretionary orogenic phase, specifically the activity of the GDSD in the Gangdese back-arc basin, we used the ^{40}Ar-^{39}Ar system to date cooling ages of white mica, plagioclase, and K-feldspar derived from mylonitic rocks that record south-vergent shearing (Fig. 7). We also performed zircon U-Pb dating on sandstone samples from the top of the Upper Cretaceous Shexing Formation to constrain the maximum depositional age and on the granites that intruded the deformational strata (Fig. 2) to constrain the minimum age of deformation.

^{40}Ar-^{39}Ar Dating Methods

Six ^{40}Ar-^{39}Ar ages were determined in two laboratories. Four samples (XY8-1-7, XJ15-3, XY10-1-1, and XY11-2-1-6) were collected from the lower

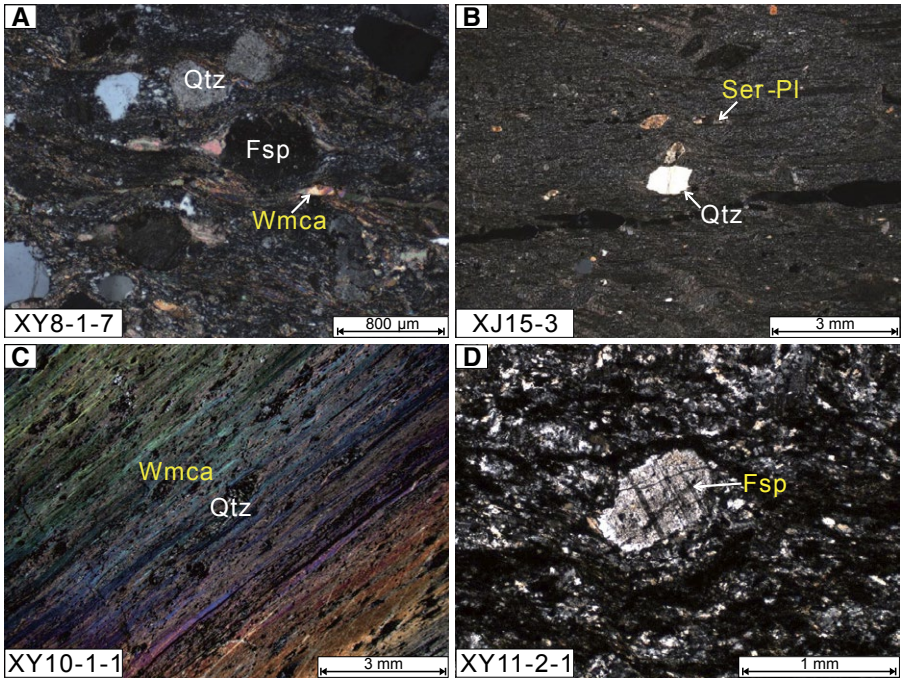

Figure 7. Photomicrographs showing the white mica (Wmca), sericitized plagioclase (Ser-Pl), and K-feldspar (Fsp) from mylonitic volcanics of the lower décollement layer of the Gangdese décollement (GDSD-1) that were selected for $^{40}Ar/^{39}Ar$ dating. (A and C) Mylonitic volcanic rock. (B) Mylonitic tuff. (D) Tuffaceous mylonite. Qtz—quartz.

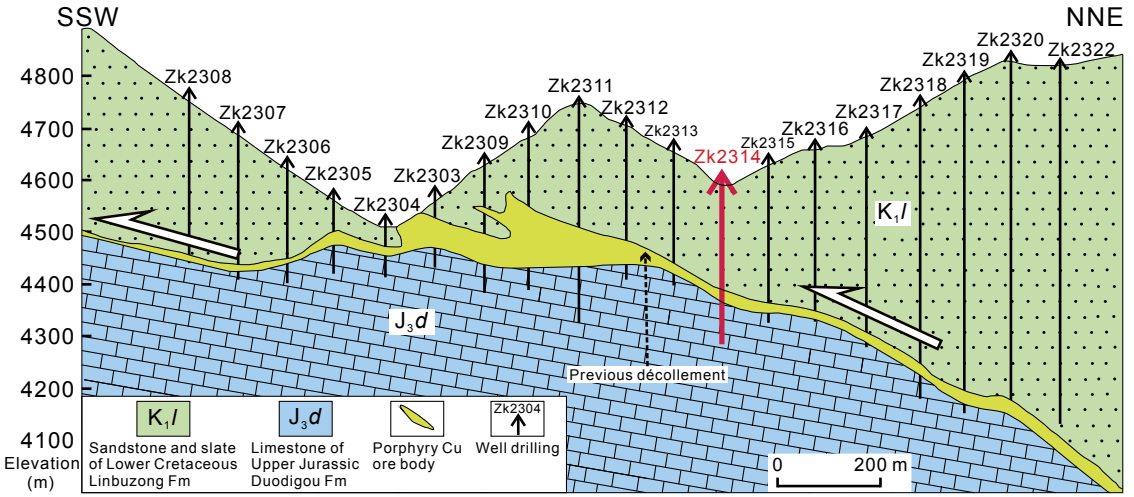

Figure 8. Cross section along drill line 23 of the Jiama mine and the location of drill core ZK2314, in the Gangdese back-arc basin, showing petrological and structural information. The core location is shown in Figure 2A. Porphyry copper ore is developed along the upper décollement layer of the Gangdese décollement (GDSD-2) between the overlying Lower Cretaceous Linbuzong Formation (K_1l) and the underlying Upper Jurassic Duodigou Formation (J_3d), as indicated by white arrows showing top-to-the-SSW shearing.

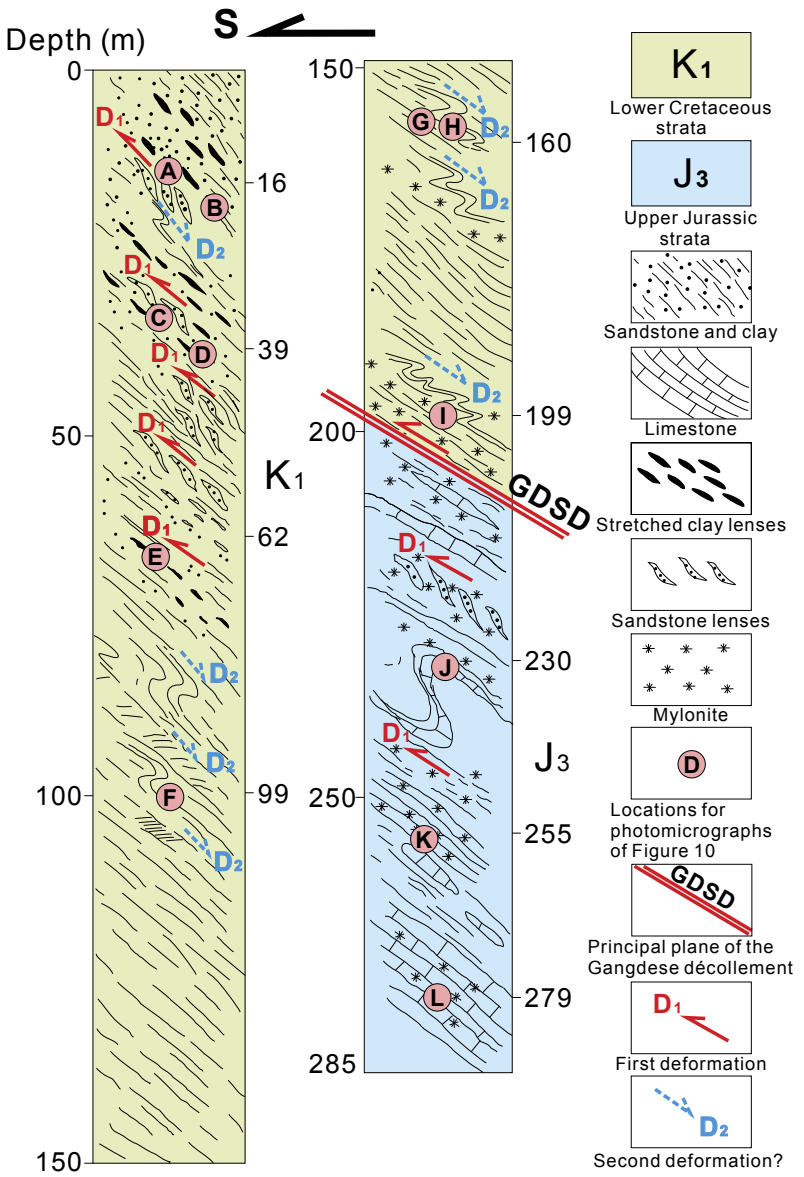

Figure 9. Synthesis of lithologic and structural data for drill core ZK2314 from the Jiama mine of the Gangdese back-arc basin (Fig. 8), showing the principal plane of the upper décollement layer of the Gangdese décollement (GDSD-2) between the lower part of the Lower Cretaceous strata and the upper part of the Upper Jurassic strata. We infer two phases of deformation with opposite senses of shear. D_1—early deformation characterized by top-to-the-south shearing; D_2—late deformation showing top-to-the-north shearing.

décollement layer of GDSD-1 (Fig. 2). Samples XY8-1-7 and XJ15-3 are classified as volcanic mylonite. Sample XY10-1-1 is a mica schist whose protolith was likely a tuffaceous volcanic rock (Fig. 7). Sample XY11-2-1-6 is a granitic stock intruded into the Upper Jurassic Duodigou Formation limestone. These four samples (XY8-1-7, XJ15-3, XY10-1-1, and XY11-2-1-6) were dated at the Noble Gas Geochronology Laboratory at the University of Melbourne, Australia. Another two samples (M16-11-6 and M16-11-8, both mylonitic sandstone) were dated at the Key Laboratory of Deep-Earth Dynamics, Ministry of Natural Resources, Institute of Geology, Chinese Academy of Geological Sciences. Detailed analytical methods of ^{40}Ar-^{39}Ar dating are presented in Text S1 (see footnote 1). Results are tabulated in Tables S1 and S2.

^{40}Ar-^{39}Ar Dating Results

^{40}Ar-^{39}Ar results produced a mix of concordant and discordant spectra, although even discordant results can be interpreted to give approximate constraints on cooling age. The white mica of sample XY-8-1-7 yields a discordant age spectrum with a decrease in apparent ages from ca. 65 to ca. 40 Ma for the first 12% of ^{39}Ar release, followed by a gradual increase to ca. 58 Ma (Fig. S2A [see footnote 1]). The sericitized plagioclase of sample XJ15-3 yields a discordant age spectrum, with ages increasing from ca. 45 to ca. 61 Ma, with some anomalously old values at the high-temperature steps (Fig. S2B). The sericite of mica schist sample XY10-1-1 yields a discordant, "hump-shaped" spectrum, with an age range of ca. 90–100 Ma (Fig. S2C). The K-feldspar of granite sample XY11-2-1-6 yields a well-defined plateau age of 58.91 ± 0.48 Ma (2σ) for the mid- to high-temperature steps (Fig. S2D).

The white mica of sample M16-11-6 yields a concordant age spectrum with a weighted plateau age of 89.04 ± 1.11 Ma, corresponding to a normal isochron age of 88.87 ± 2.03 Ma (Figs. 11A and 11B). Similarly, the white mica of sample M16-11-8 yields a weighted plateau age of 89.51 ± 1.13 Ma, indistinguishable from the normal isochron age of 88.62 ± 1.30 Ma within error (Figs. 11C and 11D).

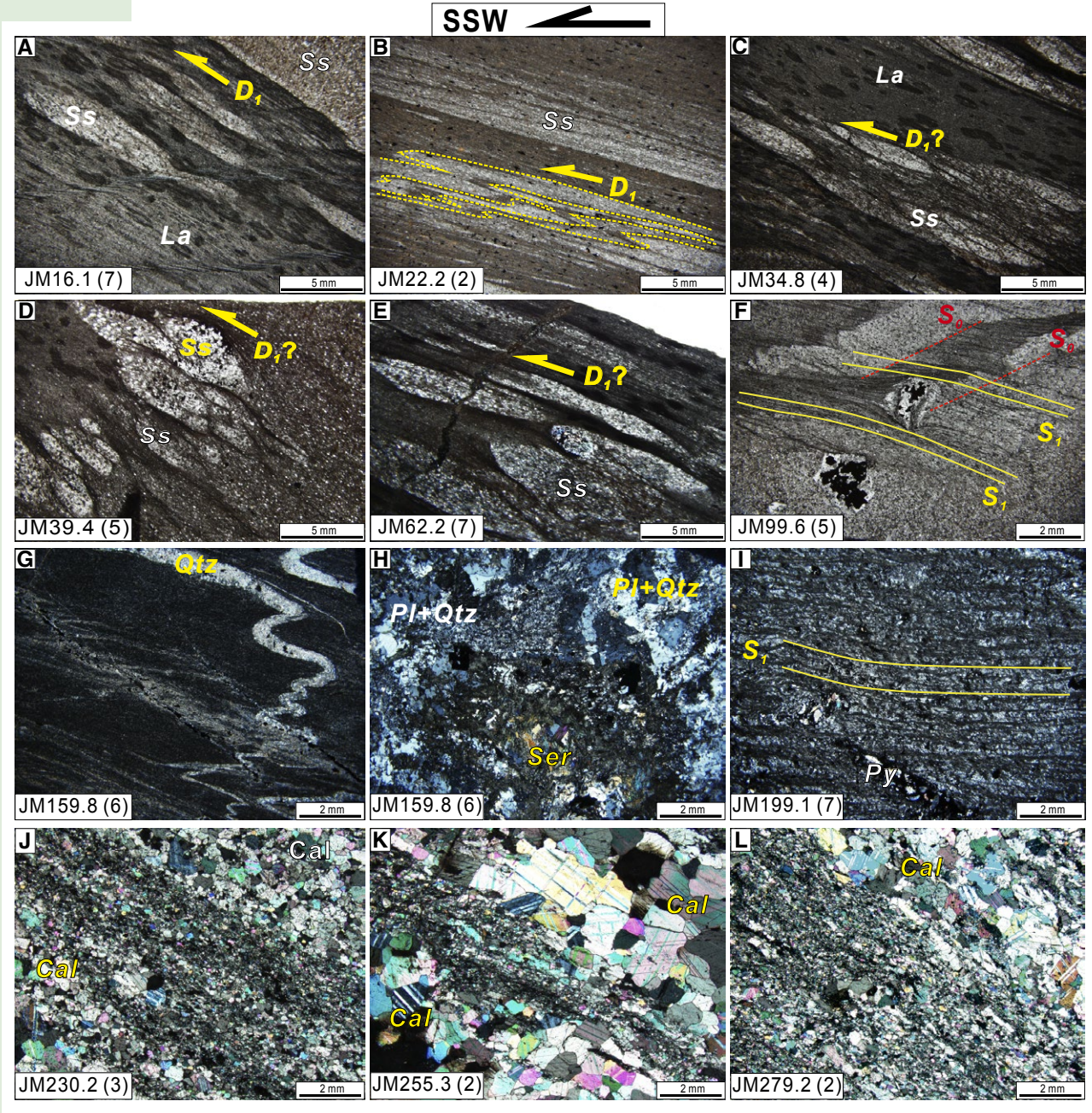

Figure 10. Photomicrographs from the ZK2314 drill core of Upper Jurassic–Lower Cretaceous sediments in the Jiama mine (Fig. 2A), showing evidence for deformation (in *X-Z* plane) from the top (16.1 m in depth) to the bottom (279 m in depth) in Lower Cretaceous Linbuzong Formation phyllite and sandstone (A–I) and in Upper Jurassic Duodigou Formation limestone (J–L). The number shown in parentheses following each sample identification label represents the thin-section number. Each sample has several thin sections. (A) S_1 with shear bands indicating top-to-the-SSW sense of shear. (B) Top-to-the-SSW sense of shear indicated by possibly shear bands in sandstone. (C–E) Shear lenses in the deformed sandstone. (F) Top-to-the-SSW sense of shear indicated by S_1 with orientation of deformed clasts. (G) Asymmetric folds. (H) Mylonitized zone of fine-grained plagioclase and quartz. (I) Late quartz + pyrite vein intruded along the foliation or spaced cleavage (S_1). (J–L) Deformed limestone of the Upper Jurassic Duodigou Formation. Cal—calcite; D_1—early deformation showing top-to-the-south shearing; La—stretching lineation shown by stretched pelitic lenses; Pl—plagioclase; Py—pyrite; Qtz—quartz; S_0—bedding; S_1—foliation of D_1; Ser—sericite; Ss—sandstone.

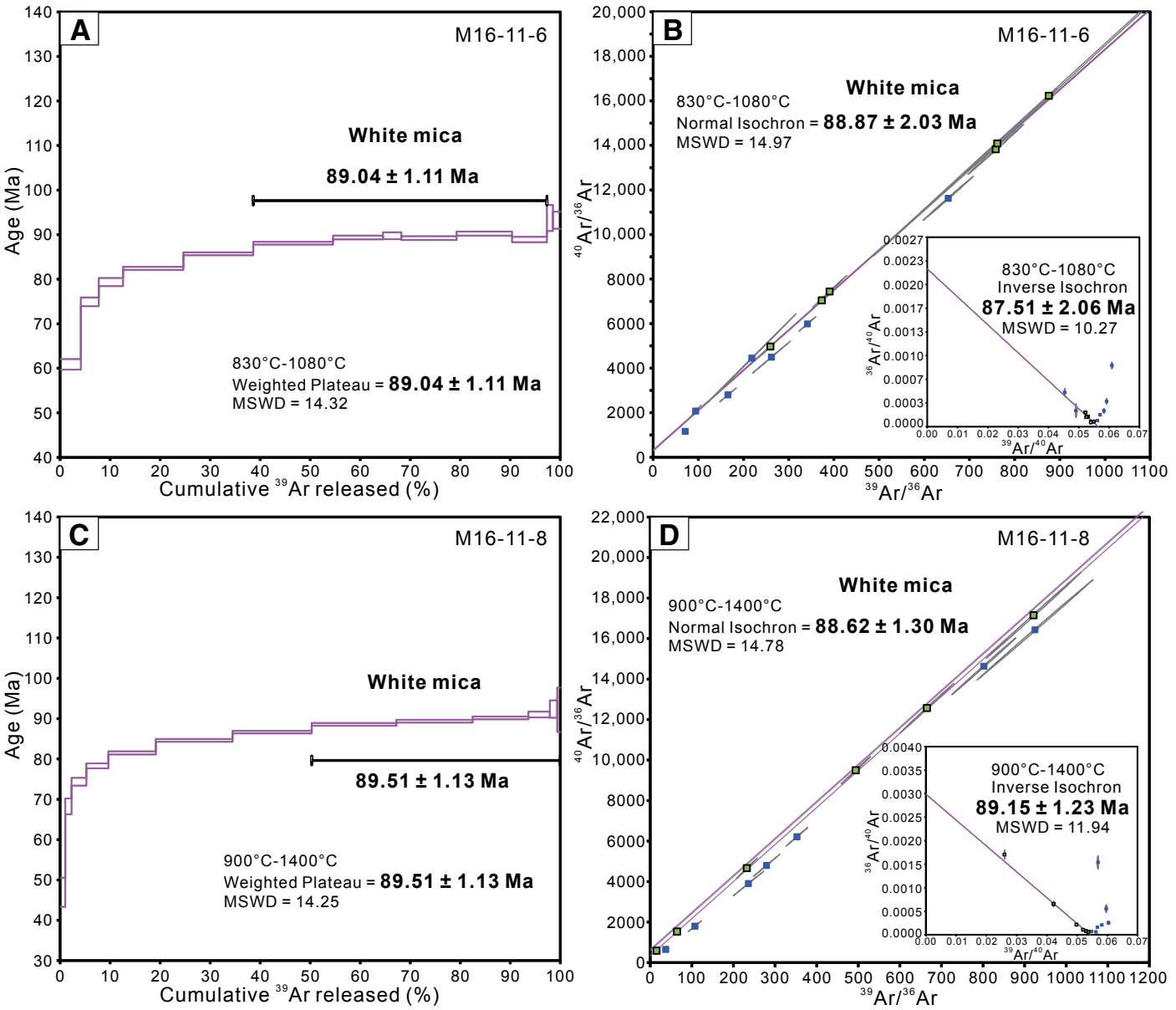

Figure 11. White mica $^{40}Ar/^{39}Ar$ plateau (A and C) and isochron (B and D) ages for samples M16-11-6 and M16-11-8 from the mylonitic sandstone of the lower décollement layer of the Gangdese décollement (GDSD-1). MSWD—mean square of weighted deviates.

Zircon U-Pb Dating Results

Detrital Zircon U-Pb Ages of the Shexing Formation Sandstone

Detailed analytical methods of zircon U-Pb dating are presented in Text S1 (see footnote 1). Sample Ct18 (sandstone) was collected from the top of the Shexing Formation, which is unconformably overlain by the 65–40 Ma volcano-sedimentary Linzizong Formation (Fig. 2; Fig. S1E). U-Pb dating of its detrital zircon grains yielded a large age range from Neoarchean to Late Cretaceous (ca. 2638–87 Ma), revealing complex provenance. The 11 youngest concordant zircon U-Pb ages yielded a weighted mean age of 91.1 ± 2.1 Ma (Fig. 12). This age is indistinguishable from the age of the youngest red beds of the Shexing Formation (ca. 90 Ma; Kapp et al., 2007; Li et al., 2015b; Wang et al., 2020; Wei et al., 2020). In Zhu et al. (2019), the youngest age group of detrital zircons from the uppermost Shexing Formation sandstone was dated at 85 ± 1 Ma, and they suggested that the strong folding and deformation of the Upper Cretaceous Shexing Formation at Maxiang took place between 85 Ma and 69 Ma. In other words, the maximum depositional age of the Shexing Formation could be no older than 85 Ma (Zhu et al., 2019), which is a little younger than the age of ca. 90 Ma from Kapp et al. (2007) and the present study. However, the calculation methods of both Zhu et al. (2019) and the present study have employed the weighted mean age of the youngest age group of detrital zircons, whose precision mainly relied on the age number, age distribution, and analytical errors. Thus, both results are reasonable and acceptable. More work is needed in the future. Tentatively, our new results, in combination with published age data, suggest that the maximum depositional age of the Shexing Formation is ca. 90 Ma. The analytical results are presented in Table S3.

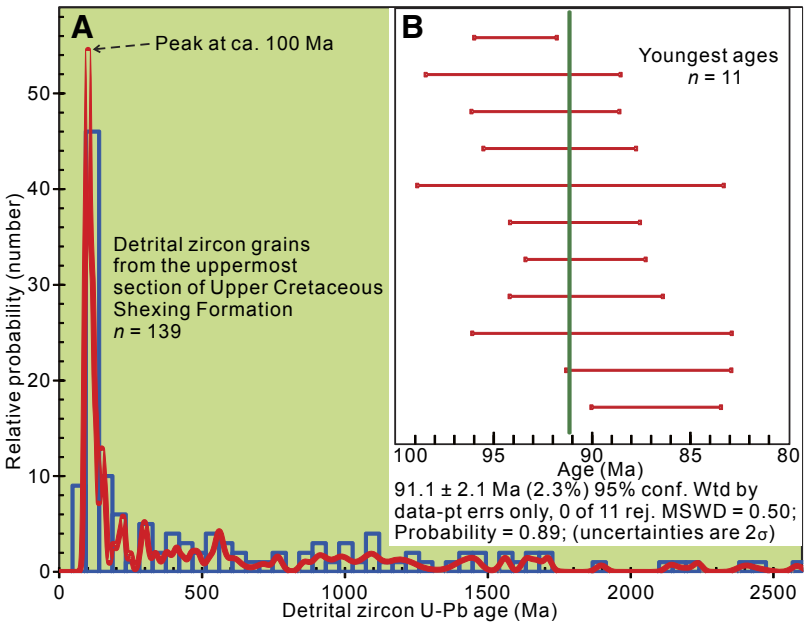

Figure 12. Detrital zircon U-Pb ages of the red bed from the top of the Shexing Formation in the Gangdese back-arc basin. A shows the complete spectrum, whereas B shows the 11 youngest grains, yielding a maximum depositional age for the Shexing Formation. Red line represents the relative probability, while the blue bars represent the bandwidth for each age range. conf.—confidence; Wtd—weighted; pt—point; errs—errors; rej.—rejected; MSWD—mean square of weighted deviates.

Zircon U-Pb Ages for Granites Intruded into the Deformed Strata

Six samples (XZ2-8-1, XZ2-8-2, XZ2-6-1, XD4-6-1, XG8-7, and XG8-8) from granites in the studied deformed strata in the Lhasa region and adjacent areas (Fig. 2) were selected for zircon U-Pb dating. Cathodoluminescence images of zircon grains from these samples show euhedral morphologies and sharp oscillatory zoning. The Th/U ratios of the zircon grains from the six samples range 0.32–0.97, 0.61–1.48, 0.39–2.14, 0.63–2.06, 0.77–1.8, and 0.52–1.32, respectively, indicating a magmatic origin (Table S4 [see footnote 1]).

U-Pb compositions (Table S4) of the zircon grains yield concordia ages of 42.2 ± 2.8 Ma (mean square of weighted deviates [MSWD] = 0.44, n = 13, sample XZ2-8-1), 66.6 ± 1.7 Ma (MSWD = 0.10, n = 15, sample XZ2-8-2), 43.7 ± 5.6 Ma (MSWD = 0.74, n = 23, sample XZ2-6-1), 48.8 ± 0.7 Ma (MSWD = 1.7, n = 16, sample XD4-6-1), 52.7 ± 0.7 Ma (MSWD = 1.2, n = 20, sample XG8-7), and 61.6 ± 1.3 Ma (MSWD = 1.3, n = 20, sample XG8-8) (Fig. 13). These data indicate that the studied granites crystallized between ca. 67 and 42 Ma, which is consistent with previous age dating results (65.6–59.3 Ma) for granites around the Lhasa region (Wen et al., 2008a; Ji et al., 2009; Zhu et al., 2015; Ma et al., 2017a) (Fig. 2).

DISCUSSION

Structural Analyses

Relationship between the Two Phases of Deformation

Based on our structural analysis, we suggest two stages of deformation: a first deformation stage (D_1) with top-to-the-south–directed shearing

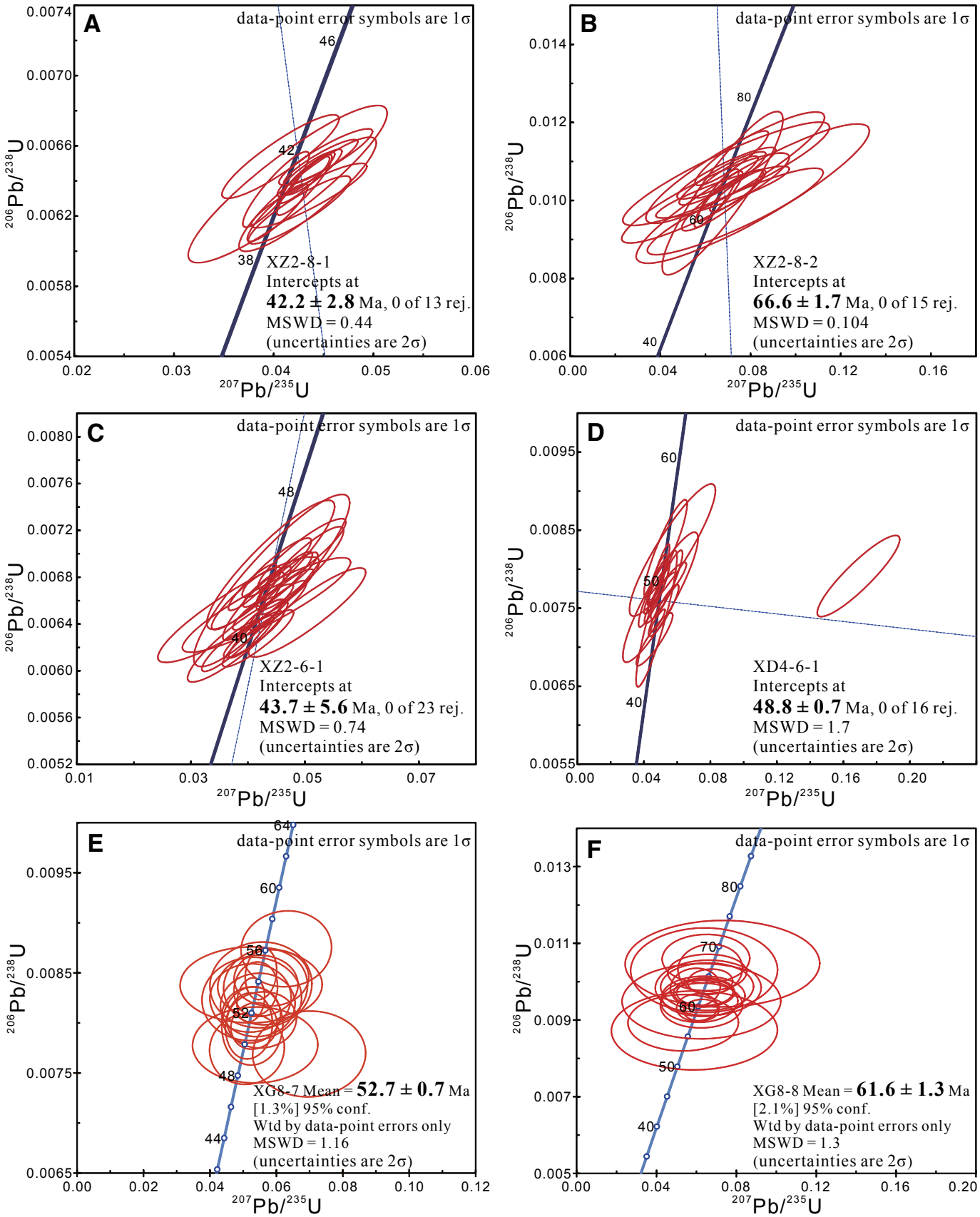

Figure 13. Zircon U-Pb concordia ages of granitic rock samples XZ2-8-1 (A), XZ2-8-2 (B), XZ2-6-1 (C), XD4-6-1 (D), XG8-7 (E), and XG8-8 (F) that intruded into the Gangdese dome structure (Fig. 2). These ages are interpreted as crystallization ages of the plutons. rej.—rejected; MSWD—mean square of weighted deviates; conf.—confidence; Wtd—weighted.

and a second deformation phase (D_2) of regional doming. D_1 records early deformation of GDSD-2, while D_2 represents regional doming, evidenced by radiating orientations of the foliation and stretching lineation (Fig. 2). As stated above, the décollements are interesting in that they do not preserve evidence for duplication of the stratigraphic section. Based on the results presented in the cross sections, we found that they do not juxtapose older rocks on younger rocks (Figs. 2 and 4). GDSD-1 is developed between the underlying volcano-sedimentary sequences of the Middle Jurassic Yeba Formation and the overlying Upper Jurassic limestone of the Duodigou Formation (Fig. 4). GDSD-2 is developed between the underlying Upper Jurassic Duodigou Formation limestone and the overlying Lower Cretaceous Linbuzong Formation slate and sandstone (Fig. 4).

D_2 open folding and dome structure may have been triggered by or otherwise related to the intrusion of the ca. 65–43 Ma granitic plutons during continuing contraction (Ma et al., 2017a), analogous to gneiss domes that are structural domes cored primarily by gneissic rocks and granite and mantled by high-grade schist and/or gneiss (Whitney et al., 2004) (Fig. 2B). Units that show D_1 structures were intruded by granites with ages of ca. 65–43 Ma (Fig. 2). The steep orientation of D_1 structures may result from steepening due to doming (Fig. 5).

The dated granitic plutons yielded crystallization ages of 65–43 Ma, falling into the interval of 65–40 Ma magmatic flare-up in the Gangdese belt (Ji et al., 2009; Zhu et al., 2019; Ma et al., 2022), represented by the Linzizong Formation volcanics and the Quxu batholith. However, no precise or specific age of the dome could be distinguished from these Ar-Ar dating results (Fig. S2 [see footnote 1]). At present, we cannot identify the precise syntectonic plutons from these dated granites due to a lack of detailed studies on the steep fabrics and the transition from magmatic to solid-state deformation in the granite. A comprehensive study of magmatic flow, submagmatic flow, and solid-state deformation, in combination of precise age dating, is needed to identify the syntectonic plutons north of Lhasa and to better understand the proposed doming in the retro-arc region of the Gangdese belt.

Relationship between Contraction-Related Gangdese Décollements and the Retro-Arc Fold-Thrust System

The Gangdese décollements are located to the south of the Gangdese retro-arc fold-thrust system, in close association with the Emei La and the Gulu-Hamu thrusts (Figs. 1B and 2). Structurally, the Gangdese décollements record a similar, top-to-the-south sense of shear as the Emei La and Gulu-Hamu thrusts. Temporally, the Gangdese décollements were formed coeval with the Emei La thrust, both active within the time range of 90–69 Ma (Kapp et al., 2007). Thus, we suggest that the south-vergent structures of the Gangdese décollements may have been part of a major south-directed retro-arc fold-thrust belt in the southern Lhasa terrane during the Late Cretaceous.

Timing Constraints on the Chilean-Type Orogeny of the Lhasa Terrane

The Gangdese unconformity, separating the overlying Paleogene–Eocene Linzizong Formation volcanic sequence and the underlying, folded Upper Jurassic to Cretaceous strata is a characteristic feature of the Gangdese back-arc basin (Fig. S1E [see footnote 1]). The Upper Jurassic–Cretaceous strata exhibit intense folding and thrusting associated with the sole décollement—the Gangdese décollement (GDSD) (Figs. 2 and 4)—while the Linzizong volcanic sequence is only weakly deformed (Fig. S1E) (Kapp et al., 2007). Our new zircon U-Pb age data from undeformed granites intruded into deformed Upper Jurassic–Cretaceous strata record crystallization at ca. 67–42 Ma (Figs. 2A and 13), indicating that the folding and thrusting (D_1) occurred before ca. 67 Ma. In addition, numerous reported ages of the Linzizong Formation volcanic rocks are equal to or younger than ca. 65 Ma (Ding et al., 2003; Mo et al., 2003; Lee et al., 2009), further supporting that the Gangdese angular unconformity predated ca. ~67–65 Ma.

The protolith ages of the volcanic mylonites of the Lower to Middle Jurassic Yeba Formation range between ca. 195 and 170 Ma (Zhu et al., 2008a; Wei et al., 2017; Liu et al., 2018; Ma et al., 2019). We propose that the ca. 100–90 Ma white mica ^{40}Ar-^{39}Ar age of mica schist sample XY10-1-1 from the top of the Yeba Formation of GDSD-1 provides an older age limit for initiation of GDSD-1 (Fig. S2). Two other mylonitic sandstone samples (M16-11-6 and M16-11-8) yielded consistent results, with plateau ages of 89.0 ± 1.1 Ma and 89.5 ± 1.1 Ma and corresponding normal isochron ages of 88.9 ± 2.0 Ma and 88.6 ± 1.3 Ma, respectively. These results further indicate that GDSD-1 was active prior to 89 Ma (Fig. 11). We interpret the younger ca. 65–40 Ma cooling ages of the two volcanic mylonitic samples (XY8-1-7 and XJ15-3) from beneath GDSD-1 have been reset by a thermal pulse related to the pluton emplacement or triggered by the continuing contraction due to the Indo-Asian collision (Ratschbacher et al., 1994).

An alternative explanation for the Late Cretaceous ^{40}Ar-^{39}Ar ages is that they record burial due to crustal thickening in the back-arc basin. In our opinion, however, this possibility should be ruled out based on the following: (1) the dated white micas come from mylonitic samples, whose protolith are Jurassic-aged volcano-sedimentary sequences (Figs. 5–7); (2) beginning at ca. 80 Ma, sediment transport to the forearc and trench decreased, which is inconsistent with significant crustal exhumation in the Gangdese batholith and the back-arc crust (Wu et al., 2010; Metcalf and Kapp, 2019); (3) our new ages of ca. 90–89 Ma are indistinguishable from previous results on the Late Cretaceous deformation of the Jurassic-aged Yeba Formation (Zhong et al., 2013; Feng et al., 2022); and (4) similarly, Ratschbacher et al. (1992) reported that a top-to-the-south to top-to-the-ESE displacement in the Gangdese belt is truncated by the Gangdese unconformity, and therefore they proposed that this deformation occurred between 90 and 60 Ma.

Based on fossil assemblage and ^{40}Ar-^{39}Ar dating, previous studies found that the base of the Shexing Formation (i.e., the folded sandstone beneath the >67–65 Ma unconformity) was deposited at ca. 110 Ma and that the youngest red sandstone was deposited at ca. 90 Ma (Kapp et al., 2007; Li et al., 2015b; Wang et al., 2020). Our new detrital zircon U-Pb age data for the Upper Cretaceous Shexing Formation red bed yielded a maximum depositional

age of ca. 91 Ma, which agrees within uncertainty with a previously published ca. 90 Ma depositional age (Kapp et al., 2007; Leier et al., 2007; Li et al., 2015b; Wang et al., 2020; Wei et al., 2020; Xing et al., 2020). In contrast, this result is older than the K-Ar age of 68–75 Ma for basalt within the Shexing Formation (Cao et al., 2017a). However, new interpretations suggest that the dated basalt intruded as a sill within the Shexing Formation (Wang et al., 2020). Deformed rocks of the Upper Jurassic to Cretaceous sequence are intruded by undeformed granites at ca. 67–42 Ma and are unconformably overlain by the Linzizong Formation volcanic sequence (65–44 Ma) (He et al., 2007; Zhu et al., 2015). Considering the Gangdese angular unconformity formed between 85 and 69 Ma (Zhu et al., 2019), we therefore infer that the Gangdese accretionary orogenic phase initiated at ca. 90 Ma, culminating between ca. 85 and 69 Ma.

The large-scale Gangdese angular unconformity has been interpreted to mark the initial collision between the Asian and Indian continents (Mo et al., 2008). Recently, an increasing number of studies have argued that the initial Indo-Asian collision occurred at 59–55 Ma (DeCelles et al., 2014; Hu et al., 2015; Zhu et al., 2019) or as late as 40–23 Ma (Aitchison et al., 2007; Ao et al., 2018; van Hinsbergen et al., 2019). Based on our structural analysis along with new and published age data, we argue that shortening along the GDSD initiated at ca. 90 Ma, followed by the formation of the ca. 85–67 Ma angular unconformity of the Lhasa terrane.

Late Cretaceous Crustal Deformation and Arc Magmatic Lull during the Accretionary Orogenic Phase

Numerous studies have found that magma addition and crustal growth have been episodic throughout Earth's history, with prominent magmatic episodes at ca. 2100–1800 Ma, 1100–800 Ma, and 350–250 Ma, corresponding to the assembly of the Columbia, Rodinia, and Pangea supercontinents, respectively (Condie, 1998, 2007; Rogers and Santosh, 2003; Kröner and Stern, 2004; Cawood and Buchan, 2007; Linnemann et al., 2008; Cao et al., 2017b; Spencer et al., 2018). Recent studies have similarly demonstrated that the construction of Phanerozoic arc belts worldwide has also been episodic, with so-called magmatic flare-ups (voluminous magma additions) typically lasting ~10–30 m.y. and intermittent magmatic lulls (minor magma additions) (Ducea and Barton, 2007; Ducea et al., 2015; Paterson and Ducea, 2015; Cao et al., 2017b; Chapman et al., 2017; Ma et al., 2021b, 2022). These magmatic tempos are thought to be controlled by deep geodynamic processes, for example, by the angle of the subducting slab and the extent of mantle wedge partial melting (DeCelles et al., 2015; Chapman and Ducea, 2019; Martínez Ardila et al., 2019).

Magmatism in the Gangdese belt is clearly episodic with magmatic flare-ups at ca. 100–80 Ma and ca. 65–45 Ma and a pronounced arc magmatic lull between ca. 80 and 65 Ma (Figs. 14 and 15) (Ji et al., 2009; Zhu et al., 2019; Ma et al., 2022). The cause of the ca. 100–80 Ma magmatic flare-up is debated, having been ascribed to either ridge subduction (Fig. 16A) (Zhang et al., 2010) or slab rollback (Ma et al., 2015). The ca. 65–45 Ma magmatic flare-up, which was volumetrically more significant than the ca. 100–80 Ma flare-up, has been attributed to slab rollback and subsequent slab breakoff, marking the transition from ocean-continent subduction to Indo-Asian continent-continent collision (Mo et al., 2003; Ma et al., 2017c). Studies documenting magmatic flare-ups of the Gangdese belt clearly document a magmatic lull between ca. 80 and 65 Ma (Figs. 14 and 15). Details of the geodynamic configuration during this magmatic lull, however, remain largely unresolved.

The Gangdese belt underwent several major evolutionary stages between the Late Cretaceous and the Eocene (Fig. 16). First, mid-ocean ridge subduction of the Neotethyan oceanic slab occurred beneath the southern Lhasa terrane between ca. 100 and 85 Ma, which triggered a magmatic flare-up with formation of voluminous intrusions and high-temperature granulite-facies metamorphism (Fig. 16A) (Zhang et al., 2010; Kapp and DeCelles, 2019; Zhu et al., 2019; Ding et al., 2022b). Second, the Gangdese accretionary orogenic phase took place at ca. 85–65 Ma. Different dating campaigns (this study; Zhong et al., 2013; Ma et al., 2017a; Zhu et al., 2019) have, however, revealed that fold-thrust and sole décollement of the Gangdese back-arc basin took place between 90 and 67 Ma, commencing prior to but temporally overlapping with the arc magmatic lull in the Gangdese belt (Wen et al., 2008a). The Gangdese belt underwent crustal shortening, thickening, uplift, and erosion, as well as a magmatic lull, plausibly caused by flat-slab subduction of young, buoyant Neotethyan oceanic lithosphere (Fig. 16B) (Kapp et al., 2007; Zhong et al., 2013; Zheng et al., 2014; Ma et al., 2017a). This implies a close relationship between the magmatic lull and synchronous crustal deformation, which we explore further in the Geodynamics of the Gangdese Accretionary Orogenic Phase section below. Eventually, the Gangdese batholith entered a contractional regime at ca. 65–45 Ma. The contraction and intrusion of granitic plutons triggered the formation of the Lhasa dome structure (Ma et al., 2017a). In the meantime, the slab front of the Neotethyan oceanic lithosphere began to roll back, which was accompanied by extension within the Gangdese back-arc region. The continuing rollback induced voluminous volcanism and southward migration of the arc-type magmatism (Fig. 16C) (Ding et al., 2003; Mo et al., 2003; Ji et al., 2009; Lee et al., 2009; Zhu et al., 2015; Ma et al., 2017c).

Geodynamics of the Gangdese Accretionary Orogenic Phase

The voluminous ca. 100–85 Ma arc magmatism in the Gangdese belt was most likely triggered by subduction of the mid-ocean ridge of the Neotethys beneath the southern Lhasa terrane rather than slab rollback (Fig. 16A). Support for the mid-ocean ridge subduction model comes from the occurrence of high-temperature granulite-facies metamorphism (Zhang et al., 2010, 2015; Guo et al., 2013; Qin et al., 2019) and contraction along the southern margin of the Lhasa terrane (Zhong et al., 2013; Ma et al., 2017a; Feng et al., 2022). Young, relatively buoyant and thick oceanic lithosphere near mid-ocean ridges has a greater effective elastic thickness and is therefore more likely to subduct at a gently dipping or flat-slab geometry (van Hunen et al., 2004; Huangfu

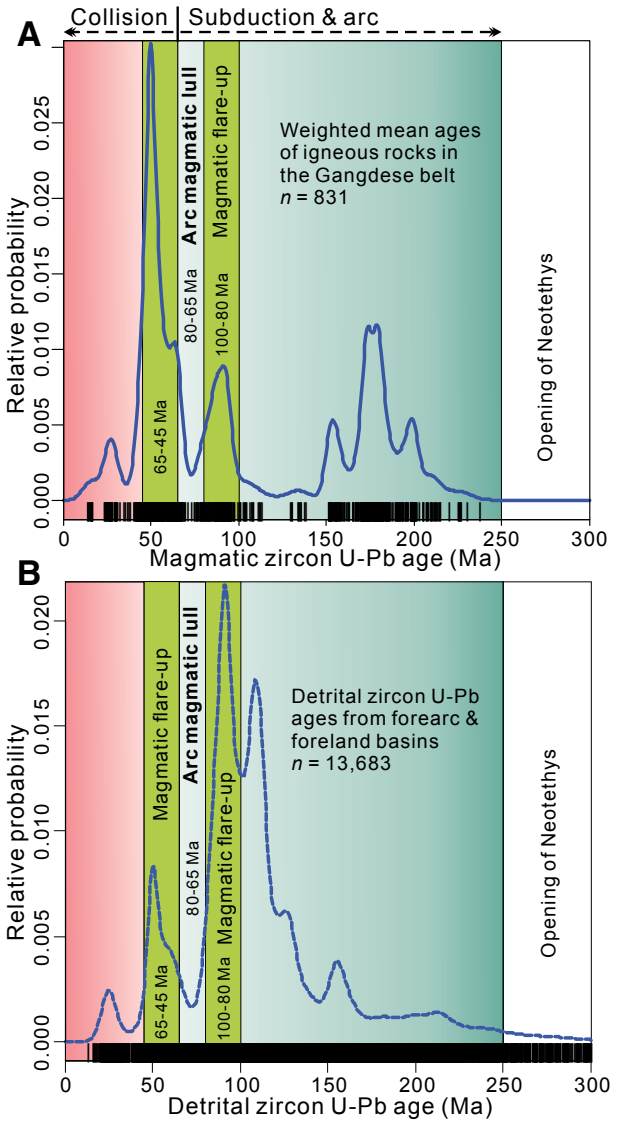

Figure 14. Kernel density estimation plots of zircon U-Pb age spectra. Black marks at the bottom represent the number density for each age range. (A) Kernel density estimation plots for zircon U-Pb weighted mean ages of the igneous rocks from the Gangdese belt. (B) Kernel density estimation plots for compiled detrital zircon U-Pb ages from trench fill, forearc and foreland basins, and modern river sands along the Indus–Yarlung Tsangpo suture zone in southern Tibet. The compiled zircon U-Pb data and corresponding references are listed in Table S5 and Table S6, respectively (see text footnote 1).

et al., 2016; Manea et al., 2017). For example, the subhorizontal slab segments below western South America are suggested to result from the subduction of relatively buoyant oceanic plateau and aseismic ridges (Martinod et al., 2010). In the Gangdese belt, the flat-slab subduction started no later than ca. 83–80 Ma, evidenced by (1) the occurrence of adakitic granitoids ca. 83–80 Ma in the Gangdese belt (Wen et al., 2008a, 2008b; Guan et al., 2010; Zheng et al., 2014; Xu et al., 2015), (2) the waning of arc magmatism from ca. 83 to 65 Ma in the Gangdese belt (Ma et al., 2022), (3) the scarcity of widespread rift-related volcanic rocks between 90 and 65 Ma (Zhu et al., 2019), (4) the cessation of the Cretaceous Takena Formation deposition at ca. 90–80 Ma (Leier et al., 2007), (5) the 85–69 Ma regional unconformity between the underlying Upper Cretaceous Shexing Formation sandstone and the overlying Paleogene Dianzhong Formation volcanic rocks in the Gangdese belt (Zhu et al., 2019), and (6) the ca. 90–69 Ma forearc and retro-arc fold-thrust system (He et al., 2007; Kapp et al., 2007).

Flat-slab subduction, in turn, may exert a traction on the overlying lithosphere, leading to contraction (Fig. 16B), as is hypothesized in Cordilleran orogens (Manea et al., 2017; Gutscher, 2018). In South America, flat-slab subduction of the Nazca plate beneath the Central Andes during the Eocene–Oligocene and beneath north-central Chile and Peru since the Pliocene has triggered uplift and deformation of the overlying crust, recorded by a series of thrusts in the forearc and back-arc regions (Ramos et al., 2002; Kay and Coira, 2009; Martinod et al., 2010; Chiarabba et al., 2016). The flattening of the subducting slab angle may thicken the crust and squeeze out the mantle wedge, a process which could initiate intrusion of adakites following the termination of arc magmatism (Fig. 16B) (Booker et al., 2004).

We show that the Gangdese belt, like the South American Cordilleran orogen (McQuarrie, 2002; Ramos, 2009), experienced folding and thrusting along the southern margin of the Lhasa terrane in the Late Cretaceous at ca. 90–65 Ma. In the forearc region, the Indus–Yarlung Tsangpo mélange was obducted southward along the south-directed thrust at ca. 63 Ma, in concert with the development

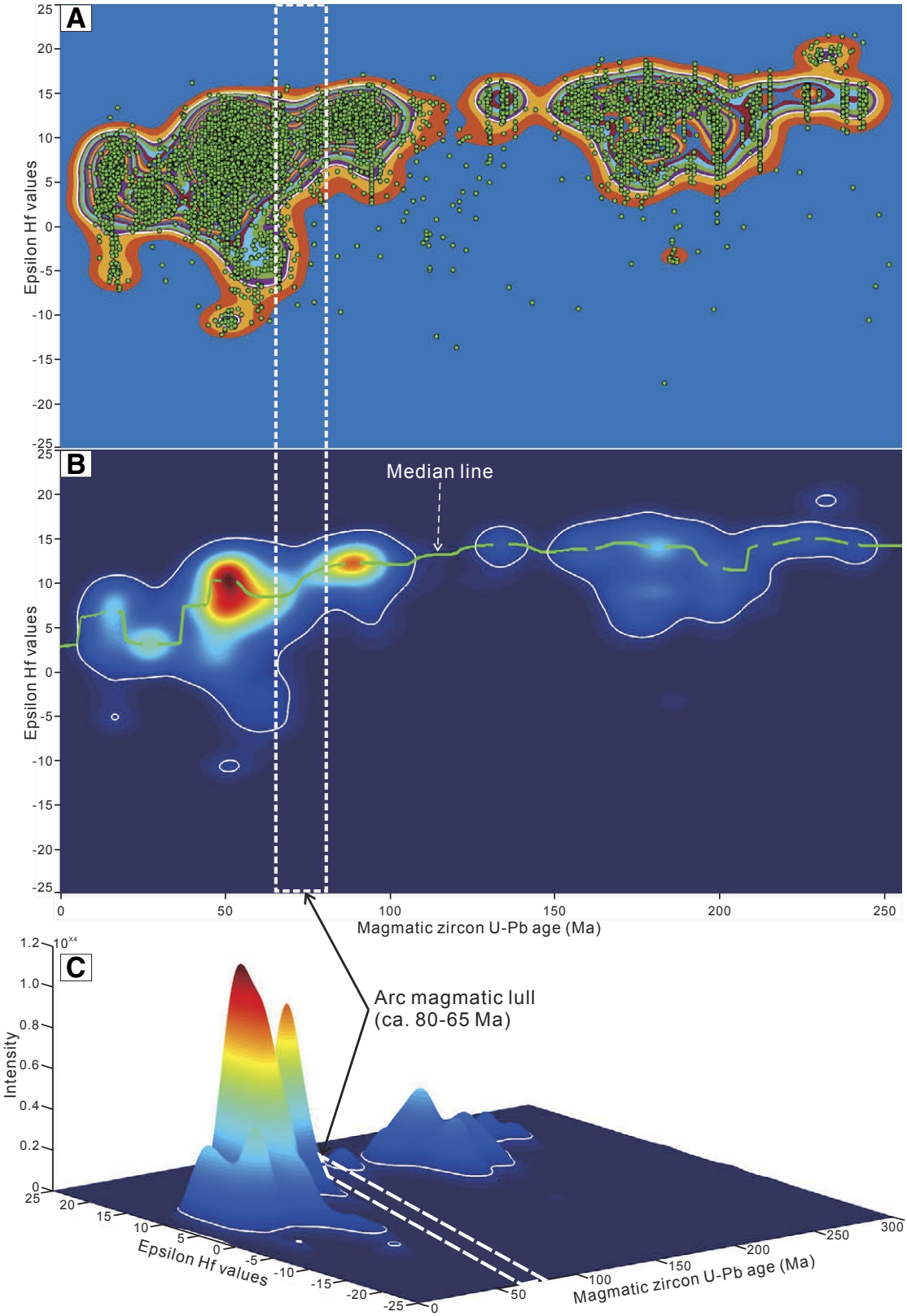

Figure 15. Distribution of magmatic zircon epsilon Hf values versus U-Pb ages (Ma). The magmatic zircon grains of igneous rocks were collected from the Gangdese magmatic belt, southern Tibet. The hafnium pattern plotting was complemented using the HafniumPlotter software (Sundell et al., 2019), which is a program designed for visualizing paired Lu-Hf geochemistry data—U-Pb geochronology as bivariate kernel density estimates (Botev et al., 2010; Sundell et al., 2019). A and B are 2-D intensity plots, while C is a 3-D intensity plot. A clearly shows the distribution of all samples, while B presents the clustering characteristics. The different colors in A represent different intensity, showing higher intensity to the core. The detailed Lu-Hf isotopic data of magmatic zircon grains from the Gangdese belt are listed in Table S7 (see text footnote 1).

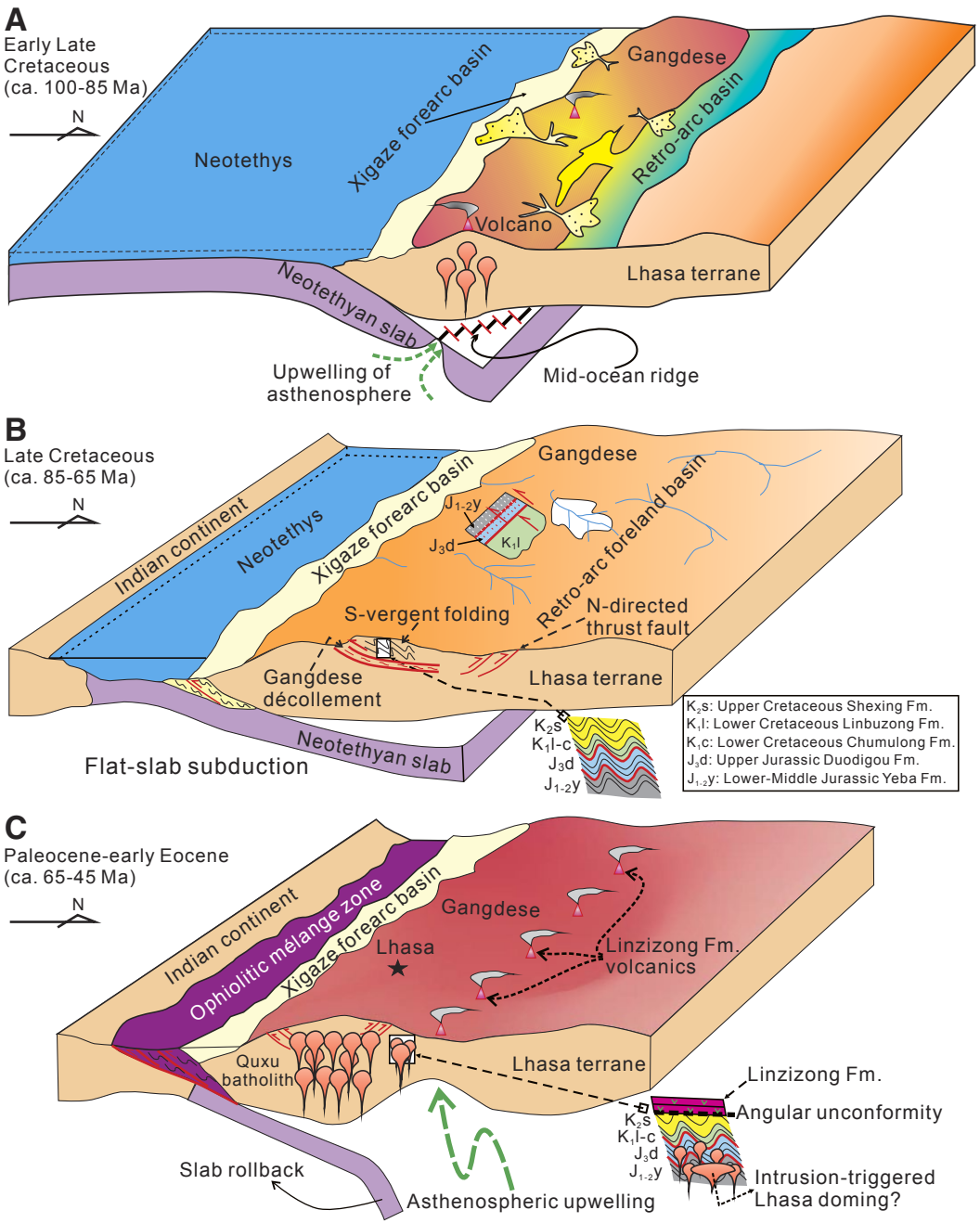

Figure 16. Schematic cartoon of tectonic models for the Late Cretaceous Gangdese accretionary orogeny related to the northward subduction of the Neotethyan oceanic lithosphere beneath the southern margin of the Lhasa terrane. (A) Ca. 100–85 magmatic flare-up in the Gangdese belt, triggered by the subduction of the Neotethyan mid-ocean ridge oceanic lithosphere beneath the Lhasa terrane. (B) Ca. 85–65 Ma crustal deformation (south-directed thrust fault and south-vergent folds, namely the Gangdese décollement) in the Gangdese belt, which could have been driven by traction from the flat-slab subduction of the Neotethyan oceanic lithosphere, during an amagmatic regime. The coeval north-directed thrust fault was delineated according to Kapp et al. (2007). (C) Ca. 65–45 Ma magmatic flare-up in the Gangdese belt, linked to the slab rollback of the Neotethyan oceanic slab. The slab rollback probably induced extension within the Gangdese retro-arc region, which caused the top-to-the-north deformation.

of an angular unconformity within the Xigaze forearc basin (between late Maastrichtian time and ca. 62 Ma) (Ding et al., 2005). To the south of the Xigaze forearc basin, a series of top-to-the-south thrusts (e.g., the Zhongba-Gyangze thrust) were active between 71 and 61 Ma (Wang et al., 2017a). Similarly, the retro-arc foreland basin of the Gangdese belt developed a series of thrusts (e.g., the Emei La thrust and Gulu-Hamu thrust), which were active between 90 and 69 Ma (Kapp et al., 2007), as well as asymmetric, north-vergent, mesoscale folding (Fig. 16B) (He et al., 2007).

The Cretaceous retro-arc basin to the north of Lhasa city was previously inferred to have been deformed from ca. 90 to 65 Ma (Ma et al., 2017a). Our new results agree with this interpretation, and we provide more constraints, including white mica ^{40}Ar-^{39}Ar dates inferred to constrain the approximate timing of deformation. We show that the angular unconformity between the overlying Linzizong Formation sequence and the underlying Shexing Formation in the Linzhou retro-arc basin developed between 90 and 67 Ma, in close agreement with constraints that suggested an unconformity age between ca. 85 and 69 Ma (Zhu et al., 2019). Our ^{40}Ar-^{39}Ar dating of white mica from mylonites along the GDSD-1 décollement yielded plateau ages of 89.5–89 Ma and corresponding 88.9–88.6 Ma isochron ages, which we interpret to indicate that top-to-the-south shearing was initiated at or before 89 Ma, immediately following (i.e., ≤1 m.y.) deposition of the Shexing Formation. The GDSD décollement is inferred to be associated with a ~2-km-thick composite sole detachment zone, exposed between the underlying Middle Jurassic Yeba Formation sequence and the overlying Upper Jurassic–Cretaceous sediments. The zones of deformation may have experienced significant slip between units. They seem more akin to detachment horizons within a fold belt rather than thrust shear zones that accommodated large amounts of shortening. The top-to-the-south GDSD décollement roots beneath the arc and carries arc rocks toward trench, which may be analogous to the West Andean thrust system, a series of structures that translate the arc westward toward the Chile trench (McQuarrie, 2002; Ramos, 2009; Díaz et al., 2014).

Subduction at low angles may induce an amagmatic regime in the overlying magmatic arc as the mantle wedge migrates in the same direction as the subducting plate (Gutscher et al., 2000; Booker et al., 2004). This plausibly occurred in the Gangdese belt, where magmatism waned from ca. 85 to 65 Ma (Fig. 14) (Wen et al., 2008a). This magmatic lull is consistent with hindered heating from the asthenospheric mantle and limited or no dehydration of the subducting slab. Accompanying the waning of the arc-type magmatism in the Gangdese belt, the Central and Northern Lhasa subterranes were gradually uplifted to the "Lhasaplano" (Kapp et al., 2007). The elevation of the "Lhasaplano" reached ~4500 m before ca. 60 Ma, corroborated by carbon and oxygen isotope data for the Nianbo Formation marls in the Linzhou Basin (Ding et al., 2014) and detrital zircon Eu/Eu* [asterisk (*) denotes square root of (Sm × Gd)] of sandstones from the Lhasa River (Tang et al., 2021).

Rollback of the Neotethyan oceanic slab front marked cessation of flat-slab subduction and induced voluminous volcanism (e.g., the Linzizong Formation volcanics) (Fig. 16C) (Wen et al., 2008a; Zhou et al., 2018). Due to slab rollback, the arc-type magmatism migrated more than ~100 km from north to south at ca. 65–50 Ma (Zhu et al., 2015, 2019), similar to migration observed in the post-orogenic magmatic province in Mesozoic South China (Li and Li, 2007) and that of the Mesozoic–Cenozoic magmatism in the western United States (Humphreys, 2009; Ardill et al., 2018). Arc magmatism flared at ca. 50 Ma (Fig. 14), forming the large-scale Quxu batholith (Fig. 16C), from which voluminous microgranular enclaves record significant input of relatively primitive magma, triggered by the subsequent slab breakoff (Dong et al., 2006; Mo et al., 2009; Ma et al., 2017c; Wang et al., 2019).

Alternatively, the relatively sparse geological observations available for the 90–70 Ma interval permit an alternative tectonic scenario along the southern Asian margin: rifting and subsequent opening of a back-arc ocean basin (Kapp and DeCelles, 2019). At present, the evidence for the rifting model comes mainly from the western Neotethyan realm, for example, the clockwise rotation and southward translation above a retreating subduction zone of the ca. 95–90 Ma Semail ophiolite of Oman prior to its obduction onto the Arabian continental margin at ca. 75 Ma (Searle et al., 2015), the generation of ca. 80–65 Ma ophiolites within suture zone between India and the Afghan block (Kakar et al., 2012), the ca. 90–80 Ma onset of southward rollback of a northward subducting slab beneath the Kohistan arc (Burg, 2011), and the ca. 90–80 Ma intra-oceanic Spong arc in the northwestern Himalaya (Pedersen et al., 2001). Some workers suggest that the Late Cretaceous north-dipping subduction zones probably extended eastward and transitioned into the retreating oceanic subduction zone beneath the Gangdese arc (Ma et al., 2013; Sundell et al., 2021). If this was the case, then the rollback of the north-dipping subducting slab would have induced upper-plate extension and led to an opening of a back-arc ocean basin, such as the proposed Xigaze back-arc basin to the north of the Xigaze arc (Kapp and DeCelles, 2019). However, there is no documented evidence for the existence of the so-called Xigaze arc in the eastern Neotethyan realm, let alone the Xigaze back-arc basin. More work is needed to examine the model of the Xigaze back-arc basin. To date, available data are most consistent with a Cordilleran-style orogenesis along the southern margin of the Lhasa terrane during the Late Cretaceous (Wen et al., 2008a; Metcalf and Kapp, 2019).

Based on our work in combination with previous studies, we suggest that the Gangdese belt could be classified as a Chilean-type advancing accretionary orogen, formed by northward flat-slab subduction of the Neotethyan oceanic lithosphere beneath the southern margin of the Asian continent during the Late Cretaceous (ca. 85–65 Ma) (Fig. 16B).

CONCLUSIONS

Structural analysis, ^{40}Ar-^{39}Ar dating, and U-Pb zircon dating reveal that a top-to-the-south décollement and associated south-vergent folds and thrusts accommodated crustal shortening, resulting in a thickened Gangdese belt during the Late Cretaceous. The timing of décollement movement, folding, and thrusting (ca. 90–67 Ma) overlaps with

the formation of the Gangdese angular unconformity (ca. 85–69 Ma) developed between lower Upper Jurassic–Cretaceous Gangdese back-arc sequences and upper Paleogene–Eocene Linzizong Formation volcanics. Moreover, published structural, geochronological, geochemical, and sedimentary data indicate that the Gangdese belt experienced an arc magmatic lull between ca. 85 and 65 Ma. Therefore, we propose that the Gangdese belt (southern Lhasa terrane) underwent a Chilean-type accretionary orogeny during the Late Cretaceous (ca. 85–65 Ma). We suggest that this accretionary orogeny was likely associated with north-directed flat-slab subduction of the Neotethyan oceanic lithosphere beneath the southern Asian continental margin.

ACKNOWLEDGMENTS

Fruitful discussions with Wenrong Cao, Weiqiang Ji, Dicheng Zhu, Andrew Laskowski, and Kate Metcalf that shed light on the accretionary orogenic phase of the Gangdese belt are much appreciated. Yuan Ma, Zhongbao Zhao, Zhihui Cai, and Huaqi Li helped us with the interpretation of structural observations. We are indebted to Associate Editor Francesco Mazzarini, reviewer Rodolfo Carosi, and an anonymous reviewer for their perceptive comments that improved this manuscript greatly. Science Editor Andrea Hampel is thanked for efficient handling and positive consideration of our work. Erdmann gratefully acknowledges support from the VOLTAIRE project (ANR-10-LABX-100-01), funded by Agence Nationale de la Recherche through the French Programme d'Investissement d'Avenir (PIA). This study was co-supported by the National Natural Science Foundation of China (grants 42272267, 42172263), the second Tibetan Plateau Scientific Expedition and Research Program (STEP) Grant (2019QZKK0901, 2019QZKK0802), the Chinese National Key Research and Development Project "Key scientific issues of transformative technology" (2019YFA0708604), the Scientific Investigation on Basic Resources program of Ministry of Science and Technology of China (2021FY100101), and the Geological Survey of China (DD20221630). Data sets for this research are available online (https://doi.org/10.5281/zenodo.7638083).

REFERENCES CITED

Aitchison, J.C., Badengzhu, Davis, A.M., Liu, J.B., Luo, H., Malpas, J.G., McDermid, I.R.C., Wu, H.Y., Ziabrev, S.V., and Zhou, M.F., 2000, Remnants of a Cretaceous intra-oceanic subduction system within the Yarlung-Zangbo suture (southern Tibet): Earth and Planetary Science Letters, v. 183, p. 231–244, https://doi.org/10.1016/S0012-821X(00)00287-9.

Aitchison, J.C., Ali, J.R., and Davis, A.M., 2007, When and where did India and Asia collide?: Journal of Geophysical Research, v. 112, B05423, https://doi.org/10.1029/2006JB004706.

Ao, S.J., Xiao, W.J., Windley, B.F., Zhang, J.E., Zhang, Z.Y., and Yang, L., 2018, Components and structures of the eastern Tethyan Himalayan Sequence in SW China: Not a passive margin shelf but a mélange accretionary prism: Geological Journal, v. 53, p. 2665–2689, https://doi.org/10.1002/gj.3103.

Ardill, K., Paterson, S., and Memeti, V., 2018, Spatiotemporal magmatic focusing in upper-mid crustal plutons of the Sierra Nevada arc: Earth and Planetary Science Letters, v. 498, p. 88–100, https://doi.org/10.1016/j.epsl.2018.06.023.

Attia, S., Cottle, J.M., and Paterson, S.R., 2020, Erupted zircon record of continental crust formation during mantle driven arc flare-ups: Geology, v. 48, p. 446–451, https://doi.org/10.1130/G46991.1.

Booker, J.R., Favetto, A., and Pomposiello, M.C., 2004, Low electrical resistivity associated with plunging of the Nazca flat slab beneath Argentina: Nature, v. 429, p. 399–403, https://doi.org/10.1038/nature02565.

Botev, Z.I., Grotowski, J.F., and Kroese, D.P., 2010, Kernel density estimation via diffusion: Annals of Statistics, v. 38, p. 2916–2957, https://doi.org/10.1214/10-AOS799.

Burg, J.-P., 2011, The Asia–Kohistan–India collision: Review and discussion, *in* Brown, D., and Ryan, P.D., eds., Arc-Continent Collision: Berlin, Heidelberg, Springer, p. 279–309, https://doi.org/10.1007/978-3-540-88558-0_10.

Cao, W.R., Lee, C.-T.A., and Lackey, J.S., 2017b, Episodic nature of continental arc activity since 750 Ma: A global compilation: Earth and Planetary Science Letters, v. 461, p. 85–95, https://doi.org/10.1016/j.epsl.2016.12.044.

Cao, Y., Sun, Z.M., Li, H.B., Pei, J.L., Jiang, W., Xu, W., Zhao, L.S., Wang, L.Z., Li, C.L., Ye, X.Z., and Zhang, L., 2017a, New Late Cretaceous paleomagnetic data from volcanic rocks and red beds from the Lhasa terrane and its implications for the paleolatitude of the southern margin of Asia prior to the collision with India: Gondwana Research, v. 41, p. 337–351, https://doi.org/10.1016/j.gr.2015.11.006.

Carosi, R., Montomoli, C., Rubatto, D., and Visonà, D., 2013, Leucogranite intruding the South Tibetan Detachment in western Nepal: Implications for exhumation models in the Himalayas: Terra Nova, v. 25, p. 478–489, https://doi.org/10.1111/ter.12062.

Carosi, R., Montomoli, C., and Iaccarino, S., 2018, 20 years of geological mapping of the metamorphic core across Central and Eastern Himalayas: Earth-Science Reviews, v. 177, p. 124–138, https://doi.org/10.1016/j.earscirev.2017.11.006.

Cawood, P.A., and Buchan, C., 2007, Linking accretionary orogenesis with supercontinent assembly: Earth-Science Reviews, v. 82, p. 217–256, https://doi.org/10.1016/j.earscirev.2007.03.003.

Chapman, J.B., and Ducea, M.N., 2019, The role of arc migration in Cordilleran orogenic cyclicity: Geology, v. 47, p. 627–631, https://doi.org/10.1130/G46117.1.

Chapman, J.B., Ducea, M.N., Kapp, P., Gehrels, G.E., and DeCelles, P.G., 2017, Spatial and temporal radiogenic isotopic trends of magmatism in Cordilleran orogens: Gondwana Research, v. 48, p. 189–204, https://doi.org/10.1016/j.gr.2017.04.019.

Chiarabba, C., De Gori, P., Faccenna, C., Speranza, F., Seccia, D., Dionicio, V., and Prieto, G.A., 2016, Subduction system and flat slab beneath the Eastern Cordillera of Colombia: Geochemistry, Geophysics, Geosystems, v. 17, p. 16–27, https://doi.org/10.1002/2015GC006048.

Chung, S.L., Chu, M.F., Zhang, Y.Q., Xie, Y.W., Lo, C.H., Lee, T.Y., Lan, C.Y., Li, X.H., Zhang, Q., and Wang, Y.Z., 2005, Tibetan tectonic evolution inferred from spatial and temporal variations in post-collisional magmatism: Earth-Science Reviews, v. 68, p. 173–196, https://doi.org/10.1016/j.earscirev.2004.05.001.

Condie, K.C., 1998, Episodic continental growth and supercontinents: A mantle avalanche connection?: Earth and Planetary Science Letters, v. 163, p. 97–108, https://doi.org/10.1016/S0012-821X(98)00178-2.

Condie, K.C., 2007, Accretionary orogens in space and time, *in* Hatcher, R.D., Jr., Carlson, M.P., McBride, J.H., and Martínez Catalán, J.R., eds., 4-D Framework of Continental Crust: Geological Society of America Memoir 200, p. 145–158, https://doi.org/10.1130/2007.1200(09).

DeCelles, P.G., Kapp, P., Gehrels, G.E., and Ding, L., 2014, Paleocene-Eocene foreland basin evolution in the Himalaya of southern Tibet and Nepal: Implications for the age of initial India-Asia collision: Tectonics, v. 33, p. 824–849, https://doi.org/10.1002/2014TC003522.

DeCelles, P.G., Zandt, G., Beck, S.L., Currie, C.A., Ducea, M.N., Kapp, P., Gehrels, G.E., Carrapa, B., Quade, J., and Schoenbohm, L.M., 2015, Cyclical orogenic processes in the Cenozoic central Andes, *in* DeCelles, P.G., Ducea, M.N., Carrapa, B., and Kapp, P.A., eds., Geodynamics of a Cordilleran Orogenic System: The Central Andes of Argentina and Northern Chile: Geological Society of America Memoir 212, p. 459–490, https://doi.org/10.1130/2015.1212(22).

Díaz, D., Maksymowicz, A., Vargas, G., Vera, E., Contreras-Reyes, E., and Rebolledo, S., 2014, Exploring the shallow structure of the San Ramón thrust fault in Santiago, Chile (~33.5° S), using active seismic and electric methods: Solid Earth, v. 5, p. 837–849, https://doi.org/10.5194/se-5-837-2014.

Ding, H.X., Zhang, Z.M., Dong, X., Tian, Z.L., Xiang, H., Mu, H.C., Gou, Z.B., Shui, X.F., Li, W.C., and Mao, L.J., 2016, Early Eocene (c. 50 Ma) collision of the Indian and Asian continents: Constraints from the North Himalayan metamorphic rocks, southeastern Tibet: Earth and Planetary Science Letters, v. 435, p. 64–73, https://doi.org/10.1016/j.epsl.2015.12.006.

Ding, H.X., Zhang, Z.M., and Kohn, M.J., 2022a, Late Cretaceous hydrous melting and reworking of juvenile lower crust of the eastern Gangdese magmatic arc, southern Tibet: Gondwana Research, v. 104, p. 112–125, https://doi.org/10.1016/j.gr.2021.07.017.

Ding, H.X., Zhang, Z.M., Palin, R.M., Kohn, M.J., Niu, Z.X., Chen, Y.F., Qin, S.K., Jiang, Y.Y., and Li, W.T., 2022b, Late Cretaceous metamorphism and anatexis of the Gangdese magmatic arc, South Tibet: Implications for thickening and differentiation of juvenile crust: Journal of Petrology, v. 63, https://doi.org/10.1093/petrology/egac017.

Ding, L., Kapp, P., Zhong, D.L., and Deng, W.M., 2003, Cenozoic volcanism in Tibet: Evidence for a transition from oceanic to continental subduction: Journal of Petrology, v. 44, p. 1833–1865, https://doi.org/10.1093/petrology/egg061.

Ding, L., Kapp, P., and Wan, X.Q., 2005, Paleocene–Eocene record of ophiolite obduction and initial India-Asia collision, south central Tibet: Tectonics, v. 24, TC3001, https://doi.org/10.1029/2004TC001729.

Ding, L., Xu, Q., Yue, Y.H., Wang, H.Q., Cai, F.L., and Li, S., 2014, The Andean-type Gangdese Mountains: Paleoelevation record from the Paleocene–Eocene Linzhou Basin: Earth and Planetary Science Letters, v. 392, p. 250–264, https://doi.org/10.1016/j.epsl.2014.01.045.

Dong, G.C., Mo, X.X., Zhao, Z.D., Zhu, D.C., Wang, L.L., Chen, T., and Li, B., 2006, Magma mixing in middle part of Gangdise magma belt: Evidences from granitoid complex: Acta Petrologica Sinica, v. 24, p. 835–844 (in Chinese with English abstract).

Dong, X., Zhang, Z.M., Klemd, R., He, Z.Y., and Tian, Z.L., 2018, Late Cretaceous tectonothermal evolution of the southern Lhasa terrane, South Tibet: Consequence of a Mesozoic Andean-type orogeny: Tectonophysics, v. 730, p. 100–113, https://doi.org/10.1016/j.tecto.2018.03.001.

Ducea, M.N., and Barton, M.D., 2007, Igniting flare-up events in Cordilleran arcs: Geology, v. 35, p. 1047–1050, https://doi.org/10.1130/G23898A.1.

Ducea, M.N., Paterson, S.R., and DeCelles, P.G., 2015, High-volume magmatic events in subduction systems: Elements, v. 11, p. 99–104, https://doi.org/10.2113/gselements.11.2.99.

Feng, Y.P., Tang, Y., Wang, G.H., Lu, Y., Li, D., Dan, C., Meng, Y.K., Zhang, P.L., Hu, J.X., and Fan, Z.Z., 2022, Kinematics, strain pattern, and temperature environment of the Yeba shear zone and multistage structural evolution of the Yeba Group: International Journal of Earth Sciences, v. 111, p. 439–461, https://doi.org/10.1007/s00531-021-02123-8.

Grujic, D., 2006, Channel flow and continental collision tectonics: An overview, *in* Law, R.D., Searle, M.P., and Godin, L., eds., Channel Flow, Ductile Extrusion and Exhumation in Continental Collision Zones: Geological Society of London Special Publication 268, p. 25–37, https://doi.org/10.1144/GSL.SP.2006.268.01.02.

Grujic, D., Ashley, K.T., Coble, M.A., Coutand, I., Kellett, D.A., Larson, K.P., Whipp, D.M., Gao, M., and Whynot, N., 2020, Deformational temperatures across the Lesser Himalayan Sequence in eastern Bhutan and their implications for the deformation history of the Main Central Thrust: Tectonics, v. 39, https://doi.org/10.1029/2019TC005914.

Guan, Q., Zhu, D.C., Zhao, Z.D., Zhang, L.L., Liu, M., Li, X.W., Yu, F., and Mo, X.X., 2010, Late Cretaceous adakites in the eastern segment of the Gangdese Belt, southern Tibet: Products of Neo-Tethyan ridge subduction?: Acta Petrologica Sinica, v. 26, p. 2165–2179 (in Chinese with English abstract).

Guo, L., Zhang, H.F., Harris, N., Pan, F.B., and Xu, W.C., 2013, Late Cretaceous (~81 Ma) high-temperature metamorphism in the southeastern Lhasa terrane: Implication for the Neo-Tethys ocean ridge subduction: Tectonophysics, v. 608, p. 112–126, https://doi.org/10.1016/j.tecto.2013.10.007.

Gutscher, M.A., 2018, Scraped by flat-slab subduction: Nature Geoscience, v. 11, p. 890–891, https://doi.org/10.1038/s41561-018-0270-x.

Gutscher, M.-A., Spakman, W., Bijwaard, H., and Engdahl, E.R., 2000, Geodynamics of flat subduction: Seismicity and tomographic constraints from the Andean margin: Tectonics, v. 19, p. 814–833, https://doi.org/10.1029/1999TC001152.

He, S.D., Kapp, P., DeCelles, P.G., Gehrels, G.E., and Heizler, M., 2007, Cretaceous–Tertiary geology of the Gangdese Arc in the Linzhou area, southern Tibet: Tectonophysics, v. 433, p. 15–37, https://doi.org/10.1016/j.tecto.2007.01.005.

Hu, X.M., Garzanti, E., Moore, T., and Raffi, I., 2015, Direct stratigraphic dating of India-Asia collision onset at the Selandian (middle Paleocene, 59 ± 1 Ma): Geology, v. 43, p. 859–862, https://doi.org/10.1130/G36872.1.

Huang, W.T., van Hinsbergen, D.J.J., Marco, M., Orme, D.A., Guillaume, D.N., Guilmette, C., Ding, L., Guo, Z.J., and Kapp, P., 2015, Lower Cretaceous Xigaze ophiolites formed in the Gangdese forearc: Evidence from paleomagnetism, sediment provenance, and stratigraphy: Earth and Planetary Science Letters, v. 415, p. 142–153, https://doi.org/10.1016/j.epsl.2015.01.032.

Huangfu, P.P., Wang, Y.J., Cawood, P.A., Li, Z.H., Fan, W.M., and Gerya, T.V., 2016, Thermo-mechanical controls of flat subduction: Insights from numerical modeling: Gondwana Research, v. 40, p. 170–183, https://doi.org/10.1016/j.gr.2016.08.012.

Humphreys, E., 2009, Relation of flat subduction to magmatism and deformation in the western United States, *in* Kay, S.M., Ramos, V.A., and Dickinson, W.R., eds., Backbone of the Americas: Shallow Subduction, Plateau Uplift, and Ridge and Terrane Collision: Geological Society of America Memoir 204, p. 85–98, https://doi.org/10.1130/2009.1204(04).

Jamieson, R.A., and Beaumont, C., 2013, On the origin of orogens: Geological Society of America Bulletin, v. 125, p. 1671–1702, https://doi.org/10.1130/B30855.1.

Ji, W.Q., Wu, F.Y., Chung, S.L., Li, J.X., and Liu, C.Z., 2009, Zircon U-Pb geochronology and Hf isotopic constraints on petrogenesis of the Gangdese batholith, southern Tibet: Chemical Geology, v. 262, p. 229–245, https://doi.org/10.1016/j.chemgeo.2009.01.020.

Jolivet, L., Faccenna, C., Agard, P., Frizon de Lamotte, D., Menant, A., Sternai, P., and Guillocheau, F., 2016, Neo-Tethys geodynamics and mantle convection: From extension to compression in Africa and a conceptual model for obduction: Canadian Journal of Earth Sciences, v. 53, p. 1190–1204, https://doi.org/10.1139/cjes-2015-0118.

Kakar, M.I., Collins, A.S., Mahmood, K., Foden, J.D., and Khan, M., 2012, U-Pb zircon crystallization age of the Muslim Bagh ophiolite: Enigmatic remains of an extensive pre-Himalayan arc: Geology, v. 40, p. 1099–1102, https://doi.org/10.1130/G33270.1.

Kang, Z.Q., Xu, J.F., Wilde, S.A., Feng, Z.H., Chen, J.L., Wang, B.D., Fu, W.C., and Pan, H.B., 2014, Geochronology and geochemistry of the Sangri Group Volcanic Rocks, Southern Lhasa Terrane: Implications for the early subduction history of the Neo-Tethys and Gangdese Magmatic Arc: Lithos, v. 200–201, p. 157–168, https://doi.org/10.1016/j.lithos.2014.04.019.

Kapp, P., and DeCelles, P.G., 2019, Mesozoic–Cenozoic geological evolution of the Himalayan-Tibetan orogen and working tectonic hypotheses: American Journal of Science, v. 319, p. 159–254, https://doi.org/10.2475/03.2019.01.

Kapp, P., DeCelles, P.G., Leier, A.L., Fabijanic, J.M., He, S., Pullen, A., Gehrels, G.E., and Ding, L., 2007, The Gangdese retroarc thrust belt revealed: GSA Today, v. 17, no. 7, p. 4–9, https://doi.org/10.1130/GSAT01707A.1.

Kay, S.M., and Coira, B.L., 2009, Shallowing and steepening subduction zones, continental lithospheric loss, magmatism, and crustal flow under the Central Andean Altiplano-Puna Plateau, *in* Kay, S.M., Ramos, V.A., and Dickinson, W.R., eds., Backbone of the Americas: Shallow Subduction, Plateau Uplift, and Ridge and Terrane Collision: Geological Society of America Memoir 204, p. 229–259, https://doi.org/10.1130/2009.1204(11).

Kellett, D.A., Grujic, D., and Erdmann, S., 2009, Miocene structural reorganization of the South Tibetan detachment, eastern Himalaya: Implications for continental collision: Lithosphere, v. 1, p. 259–281, https://doi.org/10.1130/L56.1.

Kröner, A., and Stern, R.J., 2004, Africa: Pan-African Orogeny, *in* Selley, R.C., Cocks, L.R.M., and Plimer, I.R., eds., Encyclopedia of Geology: Amsterdam, Elsevier, v. 1, p. 1–12, https://doi.org/10.1016/B0-12-369396-9/00431-7.

Labrousse, L., Hetényi, G., Raimbourg, H., Jolivet, L., and Andersen, T.B., 2010, Initiation of crustal-scale thrusts triggered by metamorphic reactions at depth: Insights from a comparison between the Himalayas and Scandinavian Caledonides: Tectonics, v. 29, TC5002, https://doi.org/10.1029/2009TC002602.

Laskowski, A.K., Kapp, P., Ding, L., Campbell, C., and Liu, X.H., 2017, Tectonic evolution of the Yarlung suture zone, Lopu Range region, southern Tibet: Tectonics, v. 36, p. 108–136, https://doi.org/10.1002/2016TC004334.

Laskowski, A.K., Kapp, P., and Cai, F.L., 2018, Gangdese culmination model: Oligocene–Miocene duplexing along the India-Asia suture zone, Lazi region, southern Tibet: Geological Society of America Bulletin, v. 130, p. 1355–1376, https://doi.org/10.1130/B31834.1.

Lee, H.Y., Chung, S.L., Lo, C.H., Ji, J.Q., Lee, T.Y., Qian, Q., and Zhang, Q., 2009, Eocene Neotethyan slab breakoff in southern Tibet inferred from the Linzizong volcanic record: Tectonophysics, v. 477, p. 20–35, https://doi.org/10.1016/j.tecto.2009.02.031.

Leier, A.L., DeCelles, P.G., Kapp, P., and Ding, L., 2007, The Takena Formation of the Lhasa terrane, southern Tibet: The record of a Late Cretaceous retroarc foreland basin: Geological Society of America Bulletin, v. 119, p. 31–48, https://doi.org/10.1130/B25974.1.

Li, X.H., and Mattern, F., 2021, Comparing the Upper Triassic deep-sea flysch of the Shannan Terrane with the coeval shallow shelf sediments of the Tethys Himalaya, southern Tibet: Acta Geologica Sinica (English edition), v. 95, p. 348–354, https://doi.org/10.1111/1755-6724.14659.

Li, X.X., Jiang, W., Liang, J.H., Zhao, Z.D., Liu, D., and Mo, X.X., 2015b, The geochemical characteristics and significance of the basalt from Shexing Formation in Linzhou basin, southern Tibet: Acta Petrologica Sinica, v. 31, p. 1285–1297 (in Chinese with English abstract).

Li, Y.L., Wang, C.S., Dai, J.G., Xu, G.Q., Hou, Y.L., and Li, X.H., 2015a, Propagation of the deformation and growth of the Tibetan–Himalayan orogen: A review: Earth-Science Reviews, v. 143, p. 36–61, https://doi.org/10.1016/j.earscirev.2015.01.001.

Li, Z.X., and Li, X.H., 2007, Formation of the 1300-km-wide intracontinental orogen and postorogenic magmatic province in Mesozoic South China: A flat-slab subduction model: Geology, v. 35, p. 179–182, https://doi.org/10.1130/G23193A.1.

Linnemann, U., Pereira, F., Jeffries, T.E., Drost, K., and Gerdes, A., 2008, The Cadomian Orogeny and the opening of the Rheic Ocean: The diachrony of geotectonic processes constrained by LA-ICP-MS U-Pb zircon dating (Ossa-Morena and Saxo-Thuringian Zones, Iberian and Bohemian Massifs): Tectonophysics, v. 461, p. 21–43, https://doi.org/10.1016/j.tecto.2008.05.002.

Liu, Z.C., Ding, L., Zhang, L.Y., Wang, C., Qiu, Z.L., Wang, J.G., Shen, X.L., and Deng, X.Q., 2018, Sequence and petrogenesis of the Jurassic volcanic rocks (Yeba Formation) in the Gangdese arc, southern Tibet: Implications for the Neo-Tethyan subduction: Lithos, v. 312–313, p. 72–88, https://doi.org/10.1016/j.lithos.2018.04.026.

Ma, L., Wang, Q., Li, Z.X., Wyman, D.A., Jiang, Z.Q., Yang, J.H., Gou, G.N., and Guo, H.F., 2013, Early Late Cretaceous (ca. 93 Ma) norites and hornblendites in the Milin area, eastern Gangdese: Lithosphere–asthenosphere interaction

during slab roll-back and an insight into early Late Cretaceous (ca. 100–80 Ma) magmatic "flare-up" in southern Lhasa (Tibet): Lithos, v. 172–173, p. 17–30, https://doi.org/10.1016/j.lithos.2013.03.007.

Ma, L., Wang, Q., Wyman, D.A., Jiang, Z.Q., Wu, F.Y., Li, X.H., Yang, J.H., Gou, G.N., and Guo, H.F., 2015, Late Cretaceous back-arc extension and arc system evolution in the Gangdese area, southern Tibet: Geochronological, petrological, and Sr-Nd-Hf-O isotopic evidence from Dagze diabases: Journal of Geophysical Research: Solid Earth, v. 120, p. 6159–6181, https://doi.org/10.1002/2015JB011966.

Ma, X.X., Xu, Z.Q., Meert, J.G., and Santosh, M., 2017b, Early Jurassic intra-oceanic arc system of the Neotethys Ocean: Constraints from andesites in the Gangdese magmatic belt, south Tibet: Island Arc, v. 26, https://doi.org/10.1111/iar.12202.

Ma, X.X., Meert, J.G., Xu, Z.Q., and Zhao, Z.B., 2017c, Evidence of magma mixing identified in the Early Eocene Caina pluton from the Gangdese Batholith, southern Tibet: Lithos, v. 278–281, p. 126–139, https://doi.org/10.1016/j.lithos.2017.01.020.

Ma, X.X., Meert, J.G., Xu, Z.Q., and Zhao, Z.B., 2019, The Jurassic Yeba Formation in the Gangdese arc of S. Tibet: Implications for upper plate extension in the Lhasa terrane: International Geology Review, v. 61, p. 481–503, https://doi.org/10.1080/00206814.2018.1434835.

Ma, X.X., Xu, Z.Q., Zhao, Z.B., and Yi, Z.Y., 2020, Identification of a new source for the Triassic Langjiexue Group: Evidence from a gabbro-diorite complex in the Gangdese magmatic belt and zircon microstructures from sandstones in the Tethyan Himalaya, southern Tibet: Geosphere, v. 16, p. 407–434, https://doi.org/10.1130/GES02154.1.

Ma, X.X., Gao, L.E., Zhao, Z.B., Chen, X.J., and Li, H.B., 2021a, Early Eocene leucocratic sill/dike swarms in the Gangdese belt, southern Tibet: Tectonic implications for Indo-Asian collision: China Geology, v. 4, p. 56–66, https://doi.org/10.31035/cg2021019.

Ma, X.X., Xu, Z.Q., Liu, F., Zhao, Z.B., and Li, H.B., 2021b, Continental arc tempos and crustal thickening: A case study in the Gangdese arc, southern Tibet: Acta Geologica Sinica, v. 95, p. 107–123 (in Chinese with English abstract).

Ma, X.X., Attia, S., Cawood, T., Cao, W.R., Xu, Z.Q., and Li, H.B., 2022, Arc tempos of the Gangdese batholith, southern Tibet: Journal of Geodynamics, v. 149, https://doi.org/10.1016/j.jog.2022.101897.

Ma, Y., Xu, Z.Q., Li, G.W., Ma, S.W., Ma, X.X., Chen, X.J., and Zhao, Z.B., 2017a, Crustal deformation of the Gangdese Cretaceous back-arc basin and formation of Proto-plateau, South Tibet: Acta Petrologica Sinica, v. 33, p. 3861–3872 (in Chinese with English abstract).

Manea, V.C., Manea, M., Ferrari, L., Orozco-Esquivel, T., Valenzuela, R.W., Husker, A., and Kostoglodov, V., 2017, A review of the geodynamic evolution of flat slab subduction in Mexico, Peru, and Chile: Tectonophysics, v. 695, p. 27–52, https://doi.org/10.1016/j.tecto.2016.11.037.

Martínez Ardila, A.M., Paterson, S.R., Memeti, V., Parada, M.A., and Molina, P.G., 2019, Mantle driven Cretaceous flare-ups in Cordilleran arcs: Lithos, v. 326–327, p. 19–27, https://doi.org/10.1016/j.lithos.2018.12.007.

Martinod, J., Husson, L., Roperch, P., Guillaume, B., and Espurt, N., 2010, Horizontal subduction zones, convergence velocity and the building of the Andes: Earth and Planetary Science Letters, v. 299, p. 299–309, https://doi.org/10.1016/j.epsl.2010.09.010.

McQuarrie, N., 2002, The kinematic history of the central Andean fold-thrust belt, Bolivia: Implications for building a high plateau: Geological Society of America Bulletin, v. 114, p. 950–963, https://doi.org/10.1130/0016-7606(2002)114<0950:TKHOTC>2.0.CO;2.

Meng, Y.K., Xu, Z.Q., Xu, Y., and Ma, S.W., 2018, Late Triassic granites from the Quxu batholith shedding a new light on the evolution of the Gangdese belt in southern Tibet: Acta Geologica Sinica (English edition), v. 92, p. 462–481, https://doi.org/10.1111/1755-6724.13537.

Meng, Y.K., Yuan, H.Q., Santosh, M., Mooney, W.D., and Guo, L., 2021, Heavy magnesium isotopes in the Gangdese magmatic belt: Implications for magmatism in the Mesozoic subduction system of southern Tibet: Lithos, v. 390–391, https://doi.org/10.1016/j.lithos.2021.106106.

Metcalf, K., and Kapp, P., 2019, History of subduction erosion and accretion recorded in the Yarlung Suture Zone, southern Tibet, *in* Treloar, P.J., and Searle, M.P., eds., Himalayan Tectonics: A Modern Synthesis: Geological Society of London Special Publication 483, p. 517–554, https://doi.org/10.1144/SP483.12.

Mo, X.X., Zhao, Z.D., Deng, J.F., Dong, G.C., Zhou, S., Guo, T.Y., Zhang, S.Q., and Wang, L.L., 2003, Response of volcanism to the India-Asia collision: Earth Science Frontiers, v. 10, p. 135–148 (in Chinese with English abstract).

Mo, X.X., Zhao, Z.D., Zhou, S., Dong, G.C., and Liao, Z.L., 2007, On the timing of India-Asia continental collision: Geological Bulletin of China, v. 26, p. 1240–1244 (in Chinese with English abstract).

Mo, X.X., Niu, Y.L., Dong, G.C., Zhao, Z.D., Hou, Z.Q., Zhou, S., and Ke, S., 2008, Contribution of syncollisional felsic magmatism to continental crust growth: A case study of the Paleogene Linzizong volcanic Succession in southern Tibet: Chemical Geology, v. 250, p. 49–67, https://doi.org/10.1016/j.chemgeo.2008.02.003.

Mo, X.X., Dong, G.C., Zhao, Z.D., Zhu, D.C., Zhou, S., and Niu, Y.L., 2009, Mantle input to the crust in Southern Gangdese, Tibet, during the Cenozoic: Zircon Hf isotopic evidence: Journal of Earth Science, v. 20, p. 241–249, https://doi.org/10.1007/s12583-009-0023-2.

Molnar, P., England, P., and Martinod, J., 1993, Mantle dynamics, uplift of the Tibetan Plateau, and the Indian monsoon: Reviews of Geophysics, v. 31, p. 357–396, https://doi.org/10.1029/93RG02030.

Murphy, M.A., Yin, A., Harrison, T.M., Durr, S.B., Chen, Z., Ryerson, F.J., Kidd, W.S.F., Wang, X., and Zhou, X., 1997, Did the Indo-Asian collision alone create the Tibetan plateau?: Geology, v. 25, p. 719–722, https://doi.org/10.1130/0091-7613(1997)025<0719:DTIACA>2.3.CO;2.

Najman, Y., Jenks, D., Godin, L., Boudagher-Fadel, M., Millar, I., Garzanti, E., Horstwood, M., and Bracciali, L., 2017, The Tethyan Himalayan detrital record shows that India–Asia terminal collision occurred by 54 Ma in the Western Himalaya: Earth and Planetary Science Letters, v. 459, p. 301–310, https://doi.org/10.1016/j.epsl.2016.11.036.

Orme, D.A., and Laskowski, A.K., 2016, Basin analysis of the Albian–Santonian Xigaze forearc, Lazi region, south-central Tibet: Journal of Sedimentary Research, v. 86, p. 894–913, https://doi.org/10.2110/jsr.2016.59.

Orme, D.A., Carrapa, B., and Kapp, P., 2015, Sedimentology, provenance and geochronology of the upper Cretaceous–lower Eocene western Xigaze forearc basin, southern Tibet: Basin Research, v. 27, p. 387–411, https://doi.org/10.1111/bre.12080.

Pan, G.T., Mo, X.X., Hou, Z.Q., Zhu, D.C., Wang, L.Q., Li, G.M., Geng, Q.R., and Liao, Z.L., 2006, Spatial-temporal framework of the Gangdese Orogenic Belt and its evolution: Acta Petrologica Sinica, v. 22, p. 521–533 (in Chinese with English abstract).

Paterson, S.R., and Ducea, M.N., 2015, Arc magmatic tempos: Gathering the evidence: Elements, v. 11, p. 91–98, https://doi.org/10.2113/gselements.11.2.91.

Pedersen, R.B., Searle, M.P., and Corfield, R.I., 2001, U–Pb zircon ages from the Spontang Ophiolite, Ladakh Himalaya: Journal of the Geological Society, v. 158, p. 513–520, https://doi.org/10.1144/jgs.158.3.513.

Qin, S.K., Zhang, Z.M., Jiang, Y.Y., Chen, Y.F., Zhang, N., and Zhang, C.Y., 2019, Metamorphic P-T path and tectonic implication of the sillimanite-garnet-biotite schist in the eastern Gangdese magmatic arc: Acta Petrologica Sinica, v. 35, p. 363–375 (in Chinese with English abstract).

Ramos, V.A., 2009, Anatomy and global context of the Andes: Main geologic features and the Andean orogenic cycle, *in* Kay, S.M., Ramos, V.A., and Dickinson, W.R., eds., Backbone of the Americas: Shallow Subduction, Plateau Uplift, and Ridge and Terrane Collision: Geological Society of America Memoir 204, p. 31–65, https://doi.org/10.1130/2009.1204(02).

Ramos, V.A., Cristallini, E.O., and Perez, D.J., 2002, The Pampean flat-slab of the Central Andes: Journal of South American Earth Sciences, v. 15, p. 59–78, https://doi.org/10.1016/S0895-9811(02)00006-8.

Ratschbacher, L., Frisch, W., Chen, C.S., and Pan, G.T., 1992, Deformation and motion along the southern margin of the Lhasa block (Tibet) prior to and during the India-Asia collision: Journal of Geodynamics, v. 16, p. 21–54, https://doi.org/10.1016/0264-3707(92)90017-M.

Ratschbacher, L., Frisch, W., Liu, G.H., and Chen, C.S., 1994, Distributed deformation in southern and western Tibet during and after the India-Asia collision: Journal of Geophysical Research, v. 99, p. 19,917–19,945, https://doi.org/10.1029/94JB00932.

Rogers, J.J.W., and Santosh, M., 2003, Supercontinents in Earth history: Gondwana Research, v. 6, p. 357–368, https://doi.org/10.1016/S1342-937X(05)70993-X.

Royden, L.H., Burchfiel, B.C., and van der Hilst, R.D., 2008, The geological evolution of the Tibetan Plateau: Science, v. 321, p. 1054–1058, https://doi.org/10.1126/science.1155371.

Searle, M.P., Waters, D.J., Garber, J.M., Rioux, M., Cherry, A.G., and Ambrose, T.K., 2015, Structure and metamorphism beneath the obducting Oman ophiolite: Evidence from the Bani Hamid granulites, northern Oman mountains: Geosphere, v. 11, p. 1812–1836, https://doi.org/10.1130/GES01199.1.

Spencer, C.J., Murphy, J.B., Kirkland, C.L., Liu, Y.B., and Mitchell, R.N., 2018, A Palaeoproterozoic tectono-magmatic lull as a potential trigger for the supercontinent cycle: Nature Geoscience, v. 11, p. 97–101, https://doi.org/10.1038/s41561-017-0051-y.

Stern, R.J., 2002, Subduction zones: Reviews of Geophysics, v. 40, 1012, https://doi.org/10.1029/2001RG000108.

Sundell, K.E., Saylor, J.E., and Pecha, M., 2019, Provenance and recycling of detrital zircons from Cenozoic Altiplano strata and

the crustal evolution of western South America from combined U-Pb and Lu-Hf isotopic analysis, *in* Horton, B.K., and Folguera, A., eds., Andean Tectonics: Amsterdam, Elsevier, p. 363–397, https://doi.org/10.1016/B978-0-12-816009-1.00014-9.

Sundell, K.E., Laskowski, A.K., Kapp, P.A., Ducea, M.N., and Chapman, J.B., 2021, Jurassic to Neogene Quantitative Crustal Thickness Estimates in Southern Tibet: GSA Today, v. 31, no. 6, p. 4–10, https://doi.org/10.1130/GSATG461A.1.

Tang, M., Ji, W.Q., Chu, X., Wu, A.B., and Chen, C., 2021, Reconstructing crustal thickness evolution from europium anomalies in detrital zircons: Geology, v. 49, p. 76–80, https://doi.org/10.1130/G47745.1.

Tapponnier, P., Xu, Z.Q., Roger, F., Meyer, B., Arnaud, N., Wittlinger, G., and Yang, J.S., 2001, Oblique stepwise rise and growth of the Tibet Plateau: Science, v. 294, p. 1671–1677, https://doi.org/10.1126/science.105978.

Uyeda, S., and Kanamori, H., 1979, Back-arc opening and the mode of subduction: Journal of Geophysical Research, v. 84, p. 1049–1061, https://doi.org/10.1029/JB084iB03p01049.

van Hinsbergen, D.J.J., Lippert, P.C., Li, S.H., Huang, W.T., Advokaat, E.L., and Spakman, W., 2019, Reconstructing Greater India: Paleogeographic, kinematic, and geodynamic perspectives: Tectonophysics, v. 760, p. 69–94, https://doi.org/10.1016/j.tecto.2018.04.006.

van Hunen, J., van den Berg, A.P., and Vlaar, N.J., 2004, Various mechanisms to induce present-day shallow flat subduction and implications for the younger Earth: A numerical parameter study: Physics of the Earth and Planetary Interiors, v. 146, p. 179–194, https://doi.org/10.1016/j.pepi.2003.07.027.

Wang, C., Ding, L., Zhang, L.Y., Kapp, P., Pullen, A., and Yue, Y.H., 2016, Petrogenesis of Middle–Late Triassic volcanic rocks from the Gangdese belt, southern Lhasa terrane: Implications for early subduction of Neo-Tethyan oceanic lithosphere: Lithos, v. 262, p. 320–333, https://doi.org/10.1016/j.lithos.2016.07.021.

Wang, H.Q., Ding, L., Cai, F.L., Xu, Q., Li, S., Fu, J.J., Lai, Q.Z., Yue, Y.H., and Li, X., 2017a, Early Tertiary deformation of the Zhongba–Gyangze Thrust in central southern Tibet: Gondwana Research, v. 41, p. 235–248, https://doi.org/10.1016/j.gr.2015.02.017.

Wang, J.G., Hu, X.M., Garzanti, E., An, W., and Liu, X.C., 2017b, The birth of the Xigaze forearc basin in southern Tibet: Earth and Planetary Science Letters, v. 465, p. 38–47, https://doi.org/10.1016/j.epsl.2017.02.036.

Wang, J.G., Hu, X.M., Garzanti, E., BouDagher-Fadel, M.K., Liu, Z.C., Li, J., and Wu, F.Y., 2020, From extension to tectonic inversion: Mid-Cretaceous onset of Andean-type orogeny in the Lhasa block and early topographic growth of Tibet: Geological Society of America Bulletin, v. 132, p. 2432–2454, https://doi.org/10.1130/B35314.1.

Wang, R.Q., Qiu, J.S., Yu, S.B., Lin, L., and Xu, H., 2019, Magma mixing origin for the Quxu intrusive complex in southern Tibet: Insights into the early Eocene magmatism and geodynamics of the southern Lhasa subterrane: Lithos, v. 328–329, p. 14–32, https://doi.org/10.1016/j.lithos.2019.01.019.

Wei, Y.Q., Zhao, Z.D., Niu, Y.L., Zhu, D.C., Liu, D., Wang, Q., Hou, Z.Q., Mo, X.X., and Wei, J.C., 2017, Geochronology and geochemistry of the Early Jurassic Yeba Formation volcanic rocks in southern Tibet: Initiation of back-arc rifting and crustal accretion in the southern Lhasa Terrane: Lithos, v. 278–281, p. 477–490, https://doi.org/10.1016/j.lithos.2017.02.013.

Wei, Y.Q., Zhao, Z.D., Niu, Y.L., Zhu, D.C., DePaolo, D.J., Jing, T.J., Liu, D., Guan, Q., and Sheikh, L., 2020, Geochemistry, detrital zircon geochronology and Hf isotope of the clastic rocks in southern Tibet: Implications for the Jurassic–Cretaceous tectonic evolution of the Lhasa terrane: Gondwana Research, v. 78, p. 41–57, https://doi.org/10.1016/j.gr.2019.08.014.

Wen, D.R., Liu, D.Y., Chung, S.L., Chu, M.F., Ji, J.Q., Zhang, Q., Song, B., Lee, T.Y., Yeh, M.W., and Lo, C.H., 2008a, Zircon SHRIMP U–Pb ages of the Gangdese Batholith and implications for Neotethyan subduction in southern Tibet: Chemical Geology, v. 252, p. 191–201, https://doi.org/10.1016/j.chemgeo.2008.03.003.

Wen, D.R., Chung, S.L., Song, B., Iizuka, Y., Yang, H.J., Ji, J.Q., Liu, D.Y., and Gallet, S., 2008b, Late Cretaceous Gangdese intrusions of adakitic geochemical characteristics, SE Tibet: Petrogenesis and tectonic implications: Lithos, v. 105, p. 1–11, https://doi.org/10.1016/j.lithos.2008.02.005.

Whitney, D.L., Teyssier, C., and Vanderhaeghe, O., 2004, Gneiss domes and crustal flow, *in* Whitney, D.L., Teyssier, C., and Siddoway, C.S., eds., Gneiss Domes in Orogeny: Geological Society of America Special Paper 380, p. 15–33, https://doi.org/10.1130/0-8137-2380-9.15.

Wu, F.Y., Ji, W.Q., Liu, C.Z., and Chung, S.L., 2010, Detrital zircon U–Pb and Hf isotopic data from the Xigaze fore-arc basin: Constraints on Transhimalayan magmatic evolution in southern Tibet: Chemical Geology, v. 271, p. 13–25, https://doi.org/10.1016/j.chemgeo.2009.12.007.

Xing, L.Y., Zhao, Z.D., Qi, N.Y., Tang, Y., Liu, D., Tong, X., Wang, Q., and Zhu, D.C., 2020, Geochemistry and petrogenesis of sandstones and their basaltic interlayers of Shexing Formation from Linzhou basin, South Tibet: Acta Petrologica Sinica, v. 36, p. 2729–2750 (in Chinese with English abstract).

Xu, W.C., Zhang, H.F., Luo, B.J., Guo, L., and Yang, H., 2015, Adakite-like geochemical signature produced by amphibole-dominated fractionation of arc magmas: An example from the Late Cretaceous magmatism in Gangdese belt, south Tibet: Lithos, v. 232, p. 197–210, https://doi.org/10.1016/j.lithos.2015.07.001.

Xu, Z.Q., Wang, Q., Pêcher, A., Liang, F.H., Qi, X.X., Cai, Z.H., Li, H.Q., Zeng, L.S., and Cao, H., 2013, Orogen-parallel ductile extension and extrusion of the Greater Himalaya in the late Oligocene and Miocene: Tectonics, v. 32, p. 191–215, https://doi.org/10.1002/tect.20021.

Yang, Z.M., Goldfarb, R., and Chang, Z.S., 2016, Generation of postcollisional porphyry copper deposits in southern Tibet triggered by subduction of the Indian continental plate, *in* Richards, J.P., ed., Tectonics and Metallogeny of the Tethyan Orogenic Belt: Society of Economic Geologists Special Publication 19, p. 279–300.

Yin, A., 2006, Cenozoic tectonic evolution of the Himalayan orogen as constrained by along-strike variation of structural geometry, exhumation history, and foreland sedimentation: Earth-Science Reviews, v. 76, p. 1–131, https://doi.org/10.1016/j.earscirev.2005.05.004.

Yin, A., and Harrison, T.M., 2000, Geologic evolution of the Himalayan-Tibetan orogen: Annual Review of Earth and Planetary Sciences, v. 28, p. 211–280, https://doi.org/10.1146/annurev.earth.28.1.211.

Yin, A., Harrison, T.M., Ryerson, F.J., Chen, W.J., Kidd, W.S.F., and Copeland, P., 1994, Tertiary structural evolution of the Gangdese thrust system, southeastern Tibet: Journal of Geophysical Research, v. 99, p. 18,175–18,201, https://doi.org/10.1029/94JB00504.

Zhang, Z.M., Zhao, G.C., Santosh, M., Wang, J.L., Dong, X., and Shen, K., 2010, Late Cretaceous charnockite with adakitic affinities from the Gangdese batholith, southeastern Tibet: Evidence for Neo-Tethyan mid-ocean ridge subduction?: Gondwana Research, v. 17, p. 615–631, https://doi.org/10.1016/j.gr.2009.10.007.

Zhang, Z.M., Xiang, H., Dong, X., Ding, H.X., and He, Z.Y., 2015, Long-lived high-temperature granulite-facies metamorphism in the Eastern Himalayan orogen, south Tibet: Lithos, v. 212–215, p. 1–15, https://doi.org/10.1016/j.lithos.2014.10.009.

Zhao, Z.B., Li, C., and Ma, X.X., 2021, How does the elevation changing response to crustal thickening process in the central Tibetan Plateau since 120 Ma?: China Geology, v. 4, p. 32–43, https://doi.org/10.31035/cg2021013.

Zheng, Y.C., Hou, Z.Q., Gong, Y.L., Liang, W., Sun, Q.Z., Zhang, S., Fu, Q., Huang, K.X., Li, Q.Y., and Li, W., 2014, Petrogenesis of Cretaceous adakite-like intrusions of the Gangdese Plutonic Belt, southern Tibet: Implications for mid-ocean ridge subduction and crustal growth: Lithos, v. 190–191, p. 240–263, https://doi.org/10.1016/j.lithos.2013.12.013.

Zhong, K.H., Yao, D., Dorji, Zheng, F.S., Xu, C.H., Huang, X.Y., Lu, B., Lei, B., Lin, J.Q., Bao, C.H., and Yan, G.Q., 2013, Structural features of Yeba Tectonite Group in Jiama (Gyama)-Qulong area of Tibet: Acta Geoscientica Sinica, v. 34, p. 75–86, https://doi.org/10.3975/cagsb.2013.01.07 (in Chinese with English abstract).

Zhou, L.M., Wang, R., Hou, Z.Q., Li, C., Zhao, H., Li, X.W., and Qu, W.J., 2018, Hot Paleocene-Eocene Gangdese arc: Growth of continental crust in southern Tibet: Gondwana Research, v. 62, p. 178–197, https://doi.org/10.1016/j.gr.2017.12.011.

Zhu, D.C., Pan, G.T., Chung, S.L., Liao, Z.L., Wang, L.Q., and Li, G.M., 2008a, SHRIMP zircon age and geochemical constraints on the origin of Lower Jurassic volcanic rocks from the Yeba Formation, Southern Gangdese, south Tibet: International Geology Review, v. 50, p. 442–471, https://doi.org/10.2747/0020-6814.50.5.442.

Zhu, D.C., Pan, G.T., Wang, L.Q., Mo, X.X., Zhao, Z.D., Zhou, C.Y., Liao, Z.L., Dong, G.C., and Yuan, S.H., 2008b, Tempo-spatial variations of Mesozoic magmatic rocks in the Gangdise belt, Tibet, China, with a discussion of geodynamic setting-related issues: Geological Bulletin of China, v. 27, p. 1535–1550 (in Chinese with English abstract).

Zhu, D.C., Wang, Q., Zhao, Z.D., Chung, S.L., Cawood, P.A., Niu, Y.L., Liu, S.A., Wu, F.Y., and Mo, X.X., 2015, Magmatic record of India-Asia collision: Scientific Reports, v. 5, https://doi.org/10.1038/srep14289.

Zhu, D.C., Wang, Q., Chung, S.L., Cawood, P.A., and Zhao, Z.D., 2019, Gangdese magmatism in southern Tibet and India–Asia convergence since 120 Ma, *in* Treloar, P.J., and Searle, M.P., eds., Himalayan Tectonics: A Modern Synthesis: Geological Society of London Special Publication 483, p. 583–604, https://doi.org/10.1144/SP483.14.